



POLITECNICO MILANO 1863

School of Industrial and Information Engineering
Master of Science in Space Engineering

Space Systems Engineering and Operations Final Report

1990-090B, Ulysses

Group 9

| | |
|-------------------|----------|
| Alessandro Biella | 10578810 |
| Francesco Botti | 10609503 |
| Matteo Capitanio | 10615632 |
| Alessandro Costa | 10583430 |
| Giorgio Crescenzo | 10865676 |
| Karim Towfick | 10856401 |

Academic year 2021-2022

Contents

| | |
|--|------------|
| Acronyms and abbreviations | I |
| List of Symbols | III |
| List of Figures | V |
| List of Tables | VI |
| 1 Mission objectives, Functionalities and Payloads | 1 |
| 1.1 Mission description | 1 |
| 1.2 Mission objectives | 2 |
| 1.3 Functionalities | 2 |
| 1.4 Payloads | 4 |
| 2 Mission analysis, phases and modes | 7 |
| 2.1 Phases and modes | 7 |
| 2.2 ConOps | 8 |
| 2.3 Mission analysis | 9 |
| 2.3.1 Launcher data | 9 |
| 2.3.2 Launch and adjustments in parking orbit | 10 |
| 2.3.3 Injection in interplanetary transfer | 10 |
| 2.3.4 Flyby of Jupiter | 11 |
| 2.3.5 OOE orbit | 12 |
| 2.4 Mission Analysis design effects | 12 |
| 2.5 Possible alternatives for the mission | 13 |
| 2.5.1 Simple change of plane maneuver | 13 |
| 2.5.2 Flyby alternatives | 13 |
| 2.6 Environmental analysis | 13 |
| 3 Propulsion s/s | 14 |
| 3.1 Subsystem description | 14 |
| 3.2 Propellant selection | 15 |
| 3.2.1 Gas production due to dissociation | 15 |
| 3.2.2 Freezing point | 15 |
| 3.3 Mission analysis ΔV s required | 16 |
| 3.4 Sizing of the tank | 16 |
| 3.5 Inertia moments and barycentre evaluation | 17 |
| 3.6 Environmental effects | 17 |
| 3.6.1 Temperature | 17 |
| 3.6.2 Zero-gravity effects | 17 |
| 3.7 Propulsion system mass and power consumption | 18 |
| 4 Tracking, Telemetry and Telecontrol s/s | 18 |
| 4.1 Subsystem description | 18 |
| 4.2 Ground Stations description and visibility | 19 |
| 4.2.1 Visibility | 19 |
| 4.3 Telemetry and tracking | 19 |
| 4.4 Sizing of the TTMTTC | 20 |
| 4.4.1 X-band | 20 |

| | | |
|----------|---|-----------|
| 4.4.1.1 | High Gain Antenna | 20 |
| 4.4.2 | S-band | 21 |
| 4.4.2.1 | Low Gain Antennas | 21 |
| 4.4.2.2 | High Gain Antenna | 21 |
| 4.5 | TTMTC mass and power consumption | 22 |
| 4.6 | Environmental effects | 23 |
| 4.6.1 | Conjunctions and Oppositions | 23 |
| 4.6.2 | Possible eclipse during Jupiter's flyby | 24 |
| 4.6.3 | Nutation | 24 |
| 4.6.4 | Doppler effect | 24 |
| 5 | Attitude Determination and Control s/s | 25 |
| 5.1 | Sensors | 25 |
| 5.2 | Accuracy requirements | 25 |
| 5.3 | Thrusters configuration | 26 |
| 5.4 | Attitude determination | 26 |
| 5.5 | Attitude analysis | 26 |
| 5.5.1 | Detumbling mode | 27 |
| 5.5.2 | Slew maneuver mode | 27 |
| 5.5.3 | Tracking mode | 27 |
| 5.6 | AOCS results | 27 |
| 5.6.1 | Angular velocity | 27 |
| 5.6.2 | Pointing error | 28 |
| 5.6.3 | ΔV | 29 |
| 5.7 | Possible alternatives | 30 |
| 5.7.1 | Reaction wheels and CMGs | 30 |
| 5.7.2 | Ion thrusters | 30 |
| 6 | Electrical power s/s | 30 |
| 6.1 | Subsystem description | 30 |
| 6.1.1 | RTG | 30 |
| 6.1.2 | IPDs and EPDs | 31 |
| 6.1.3 | Platform heaters | 31 |
| 6.1.3.1 | Hot case heater | 32 |
| 6.1.3.2 | Cold case heater | 32 |
| 6.1.3.3 | X-wing heater | 32 |
| 6.1.3.4 | Longeron heater | 32 |
| 6.2 | RTG power decay | 32 |
| 6.2.1 | RTG performances estimation | 33 |
| 6.2.2 | Mass of ^{238}Pu estimation | 34 |
| 6.3 | EPS power budget | 35 |
| 7 | Thermal control s/s | 35 |
| 7.1 | Multi-layer insulation | 35 |
| 7.2 | Temperature estimation | 36 |
| 7.2.1 | Transfer orbit | 36 |
| 7.2.1.1 | Hot-case scenario | 36 |
| 7.2.1.2 | Cold-case scenario | 36 |
| 7.2.2 | OOE | 37 |
| 7.3 | Results | 37 |

| | | |
|----------|--|-----------|
| 8 | On board data handling s/s | 38 |
| 8.1 | Subsystem description | 38 |
| 8.2 | Memory storage sizing | 39 |
| 8.3 | Environmental criticality | 39 |
| 9 | Configuration and Structure s/s | 40 |
| 9.1 | Configuration description | 40 |
| 9.1.1 | Spacecraft configuration | 40 |
| 9.1.2 | Launch configuration | 41 |
| 9.2 | Spacecraft structure | 42 |
| 9.3 | Structural analysis | 42 |
| 9.4 | CAD Model and Simulation results | 43 |
| R | Requirements | i |
| R.1 | Functional | i |
| R.2 | Operational | ii |
| R.3 | Performance | iii |
| A | Appendix | iv |
| A.1 | Ulysses' Timeline | iv |
| A.2 | Payloads' mass, power and data-rate budgets | v |
| A.3 | Ulysses' trajectory from ephemerides | vi |
| A.4 | Parking orbit and injection into the transfer to Jupiter | vi |
| A.5 | Earth-Jupiter transfer | vii |
| A.6 | Jupiter's flyby trajectory | vii |
| A.7 | Mars flyby alternative | viii |
| A.8 | Propellant mass and tank's temperature variability with time | ix |
| A.9 | Antennas position | ix |
| A.10 | Conjunctions and oppositions summary | x |
| A.11 | Antennas diameters sizing | xi |
| A.12 | DSN coverage | xii |
| A.13 | Radioisotopes characteristics | xii |
| A.14 | Eclipse from Jupiter | xiii |
| A.15 | External configuration of the spacecraft | xiii |
| A.16 | Upper and lower case configuration | xiv |
| A.17 | Bill of materials of figures A.12, A.13 and A.14 | xv |

Acronyms and abbreviations

| | |
|----------|---|
| AOCS | Attitude and Orbit Control System |
| AT | Anisotropy Telescopes |
| BOM | Begin Of Mission |
| CEM | Channel Electron Multipliers |
| COM | Centre Of Mass |
| CONSCAN | Conical Scan |
| COSPIN | Cosmic-ray and Solar Particle Investigation |
| CTU | Central Terminal Unit |
| CTU2 | Central Terminal Unit 2 |
| DNEL | Disconnect Non-Essential Loads |
| DSN | Deep Space Network |
| DUST | Dust Experiment |
| EOM | End Of Mission |
| EPAC/GAS | Energetic Particle Composition Experiment/Interstellar Neutral Gas Experiment |
| EPD | External Power Damper |
| EPS | Electrical Power Subsystem |
| ESA | European Space Agency |
| ESTRACK | European Space Tracking |
| ET | External Tank |
| FES | Fast Envelope Sample |
| FFT-DPU | Fast Fourier Transform Data Processing Unit |
| FGM/VHM | Flux Gate Magnetometer/Vector Helium Magnetometer |
| GRB | Gamma-Ray Burst Experiment |
| GS | Ground Station |
| HET | High Energy Telescopes |
| HFT | High Flux Telescope |
| HGA | High Gain Antenna |
| HI-SCALE | Heliosphere Instrument for Spectra Composition and Anisotropy at Low Energies |
| IPD | Internal Power Damper |
| IUS | Inertial Upper Stage |
| LGA-F | Low Gain Antenna - Forward |
| LGA-R | Low Gain Antenna - Rear |
| ISPM | International Solar-Polar Mission |
| JPL | Jet Propulsion Laboratory |
| KET | Kiel Electron Telescope |
| LET | Low Energy Telescope |
| NASA | National Aeronautics and Space Administration |
| OBDH | On Board Data Handling |
| OOE | Out Of Ecliptic |
| OP | Orbital parameters |
| PAM-S | Payload Assist Module-Special |
| PFR | Plasma Frequency Receiver |
| PS | Propulsion Subsystem |
| RAR | Radio Astronomy Receivers |
| RCS | Reaction Control System |
| RFDU | Radio Frequency Distribution Unit |
| RHCP | Right Hand Circular Polarization |
| RTG | Radioisotope Thermoelectric Generator |

| | |
|--------|---|
| SOI | Sphere Of Influence |
| SRB | Solid Rocket Booster |
| STS | Space Transportation System |
| SWICS | Solar Wind Ion Composition Spectrometer |
| SWOOPS | Solar Wind Observations Over the Poles of the Sun |
| S/C | Spacecraft |
| TCS | Thermal Control Subsystem |
| TMTTC | Tracking Telemetry and Telecontrol |
| TOF | Time Of Flight |
| TWTA | Travelling-Wave-Tube Amplifiers |
| URAP | Unified Radio and Plasma-Wave Experiment |
| GWE | Gravitational Wave Experiment |
| SCE | Solar Corona Experiment |
| WFM | Wave Form Analyzer |

List of Symbols

| Greek Symbols | | A_e | Emitting surface | [m ²] |
|----------------------|---|------------------------------------|-------------------|---|
| α | Absorbivity | [adim.] | A_{rad} | Area of the radiator [m ²] |
| ΔV | Change in velocity | [km/s] | B | Bandwidth [Hz] |
| δ | Diedral angle | [rad] | B | Blowdown ratio [adim] |
| ϵ | Emissivity | [adim.] | BER | Bit Error Rate [adim.] |
| ϵ_{\oplus} | Earth's emissivity | [adim.] | $DSN\%$ | Deep Space Network coverage [%] |
| ϵ_{rad} | Emissivity of the radiator | [adim.] | E | Energy of a particle [eV] |
| γ | Flight path angle | [rad] | e | Eccentricity [adim] |
| λ | Radioisotope decay constant | [1/years] | $EIRP$ | Equivalent Isotropic Radiated Power [dB] |
| μ | Gravitational parameter | [km ³ /s ²] | f | Frequency [Hz] |
| ν | True anomaly | [rad] | g_0 | Gravitational acceleration on Earth's surface [m/s ²] |
| Ω | Right ascension of the ascending node | [rad] | G_{rx} | Gain of the antenna in reception [dB] |
| ω | Argument of pericenter | [rad] | G_{tx} | Gain of the antenna in transmission [dB] |
| Φ | Solar constant | [W/m ²] | h_{po} | Height of the parking orbit [km] |
| ρ | Density | [kg/m ³] | i | Inclination [rad] |
| σ | Stephan-Boltzmann constant | [W/m ² K ⁴] | I_{sp} | Gravimetric specific impulse [s] |
| σ_y | Yield stress | [MPa] | k | Gain coefficient [adim.] |
| τ | Half time of a radioisotope | [years] | L_{\odot} | Solar luminosity [W] |
| Latin Symbols | | m_0 | Initial mass [kg] | |
| \bar{R} | Specific gas constant | [J/kg K] | m_f | Final mass [kg] |
| a | Semi-major axis | [km] | m_{gas} | Mass of pressurizing gas [kg] |
| A_{\oplus} | Surface subject to Earth's albedo | [m ²] | m_{prop} | Mass of propellant [kg] |
| a_{\oplus} | Albedo factor of Earth | [adim.] | m_{tank} | Mass of the tank [kg] |
| A_{\odot} | Surface subject to Sun's radiation | [m ²] | P | Electrical power [W] |
| A_{IR} | Surface subject to Earth's IR radiation | [m ²] | p_{burst} | Burst pressure [bar] |
| | | | $p_{gas,f}$ | Final pressure of pressurizing gas [bar] |

| | | | | | |
|--------------|--------------------------------------|-------|----------------------------|------------------------------------|----------------------|
| $p_{gas,i}$ | Initial pressure of pressurizing gas | [bar] | t_{tank} | Thickness of tank | [mm] |
| $p_{tank,i}$ | Initial pressure of tank | [bar] | $V_{gas,f}$ | Final volume of pressurizing gas | [m ³] |
| Q | Thermal power | [W] | $V_{gas,i}$ | Initial volume of pressurizing gas | [m ³] |
| q | Electrical charge | [C] | V_{prop} | Volume of propellant | [kg/m ³] |
| Q_{heater} | Power of the heater | [W] | V_{tank} | Volume of the tank | [m ³] |
| R_{\oplus} | Mean Earth radius | [km] | Z | Atomic number | [adim.] |
| r_{tank} | Radius of tank | [m] | Other Symbols | | |
| SEP | Sun Earth Probe angle | [deg] | \oplus | Earth | |
| SPE | Sun Probe Earth angle | [deg] | \mathcal{J} | Jupiter | |
| T | Temperature | [K] | \mathcal{M} | Mars | |
| T_{\oplus} | Black body temperature of Earth | [K] | \odot | Sun | |
| T_{burn} | Time of burn | [s] | \mathcal{V} | Venus | |
| T_{max} | Maximum acceptable temperature | [°C] | Vectors and Tensors | | |
| T_{min} | Minimum acceptable temperature | [°C] | \mathbf{A} | Attitude matrix | [3x3] |
| T_{sc} | Temperature of the spacecraft | [°C] | \mathbf{I} | Identity matrix | [3x3] |
| T_{space} | Temperature of space | [°C] | $\vec{\omega}$ | Angular velocity | [rad/s] |
| $T_{tank,i}$ | Initial tank temperature | [K] | $\vec{\omega}_d$ | Desired angular velocity | [rad/s] |
| | | | \vec{M} | Torque | [N·m] |

List of Figures

| | | |
|------|--|------|
| 1.1 | Out of Ecliptic orbit | 1 |
| 1.2 | Objectives and Functionalities | 3 |
| 1.3 | Functionalities and Requirements | 3 |
| 1.4 | Overview of the instruments locations on the Ulysses spacecraft in launch configuration | 4 |
| 2.1 | Phases and Modes | 8 |
| 2.2 | ConOps gantt | 8 |
| 2.3 | ConOps scheme | 9 |
| 2.4 | Pork-chop plot for the Earth-Jupiter arc | 11 |
| 2.5 | Ground track during a Polar passes | 12 |
| 3.1 | Architecture propulsion system | 14 |
| 3.2 | Center of mass and inertia moments variation with time cause by depletion of the propellant | 17 |
| 4.1 | Conjunctions and oppositions | 23 |
| 4.2 | Nutation and CONSCAN maneuvers | 24 |
| 5.1 | Position of Sun Sensors | 25 |
| 5.2 | Angular velocity components variation with time | 28 |
| 5.3 | Pointing error variation with time | 28 |
| 5.4 | ΔV variation with time | 29 |
| 6.1 | Estimated RTG power output with time | 34 |
| 8.1 | OBDH architecture scheme | 38 |
| 9.1 | CAD Assembly of the S/C in launch configuration | 40 |
| 9.2 | Representation of the S/C in flight configuration, from NASA 3D Resources | 41 |
| 9.3 | Comparison between the dynamic envelope and the maximum dimensions | 41 |
| 9.4 | Load configuration during launch phase | 42 |
| 9.5 | Factor of Safety from the FEM analysis | 43 |
| A.1 | Trajectory extrapolated from Ulysses' ephemerides from 1990-10-07 to 2009-06-30 | vi |
| A.2 | Parking orbit and injection into the transfer to Jupiter | vi |
| A.3 | Earth-Jupiter transfer trajectory | vii |
| A.4 | Jupiter's flyby trajectory | vii |
| A.5 | Pork-chop plot for hypothetical Earth-Mars arc | viii |
| A.6 | Hypothetical Mars' flyby | viii |
| A.7 | Antennas summary | ix |
| A.8 | Diameter of the HGA with respect to the carrier signal to noise for the communication with DSN in the X band | xi |
| A.9 | Diameter of the HGA with respect to the carrier signal to noise for the communication with DSN in the S-band | xi |
| A.10 | DSN coverage | xii |
| A.11 | Eclipse from Jupiter analysis | xiii |
| A.12 | Configuration of the external space of the S/C | xiii |
| A.13 | Configuration of the upper shelf of the case | xiv |
| A.14 | Configuration of the lower shelf of the case | xiv |

List of Tables

| | | |
|-----|--|-----|
| 1.1 | Objectives and constraints associated to every single payload | 7 |
| 2.1 | Stages and related ΔV s | 10 |
| 3.1 | Ulysses' thrusters specifications | 15 |
| 3.2 | ΔV s from the mission analysis | 16 |
| 3.3 | Sizing quantities of the Propulsion Subsystem | 16 |
| 3.4 | Estimated mass and power consumption of each component | 18 |
| 4.1 | Communication subsystem summary | 18 |
| 4.2 | Tracking data rates | 19 |
| 4.3 | Assumed parameters for the sizing of the HGA | 20 |
| 4.4 | Sized values for the HGA in X-band | 20 |
| 4.5 | Assumed parameters for the sizing of the LGA | 21 |
| 4.6 | Sized values for the LGA in S-band | 21 |
| 4.7 | Sized values for the HGA in X-band | 22 |
| 4.8 | Estimated mass and power consumption of each TTMTCS/s component | 22 |
| 5.1 | Main results of the attitude analysis | 30 |
| 6.1 | RTG electric power requirements | 33 |
| 6.2 | Mass of plutonium estimation results | 34 |
| 6.3 | Power budget for each phase compared to the RTG's power output | 35 |
| 7.1 | Temperature requirements and relative margins | 36 |
| 7.2 | Equilibrium temperatures for each phase | 37 |
| 7.3 | Radiation and heaters sizing | 38 |
| 8.1 | Telemetry data and memory storage sizing | 39 |
| A.1 | Ulysses' timeline | iv |
| A.2 | Payloads brief description | v |
| A.3 | Propellant mass stored and tank temperature during Ulysses' lifetime | ix |
| A.4 | Conjunctions timeline | x |
| A.5 | Opposition timeline | x |
| A.6 | Different radioisotopes characteristics | xii |
| A.7 | Bill of materials of figures A.12, A.13 and A.14 | xv |

1 Mission objectives, Functionalities and Payloads

1.1 Mission description

Ulysses was a joint mission between NASA and ESA which had the goal to survey the space environment above and below the poles of the Sun. More specifically the main interest was to characterize the three-dimensionality of the heliosphere by placing the spacecraft in an OOE orbit achieved thanks to gravity assist on Jupiter. Previous missions such as Mariner 10 and Pioneer 11 demonstrated that it was possible to perform a gravity assist and a spacecraft could survive in high radiation areas, such as Jupiter's neighbourhood.

The spacecraft was originally named Odysseus, because of its lengthy and indirect trajectory to study the solar poles. It was renamed Ulysses, the Latin translation of "Odysseus", at ESA's request in honor not only of Homer's mythological hero but also of Dante's character in the Inferno. Ulysses was originally scheduled for launch in May 1986 aboard the Space Shuttle Challenger. Due to the loss of Challenger, the launch of Ulysses was delayed until 6 October 1990 aboard Space Shuttle Discovery.

The initial concept of the mission called International Solar-Polar Mission (ISPM) included two spacecrafts, one European and one American, flying in formation towards Jupiter and then heading over opposite poles of the Sun which would make possible to have a simultaneous coverage of different parts of the Sun. In the 80s, due to NASA concentrating on the Space Shuttle, financial cutbacks were made in other areas of the space programme including the second spacecraft. In the end Ulysses turned into a single-spacecraft mission, using a European spacecraft with half of the instrumentation on board from the United States.

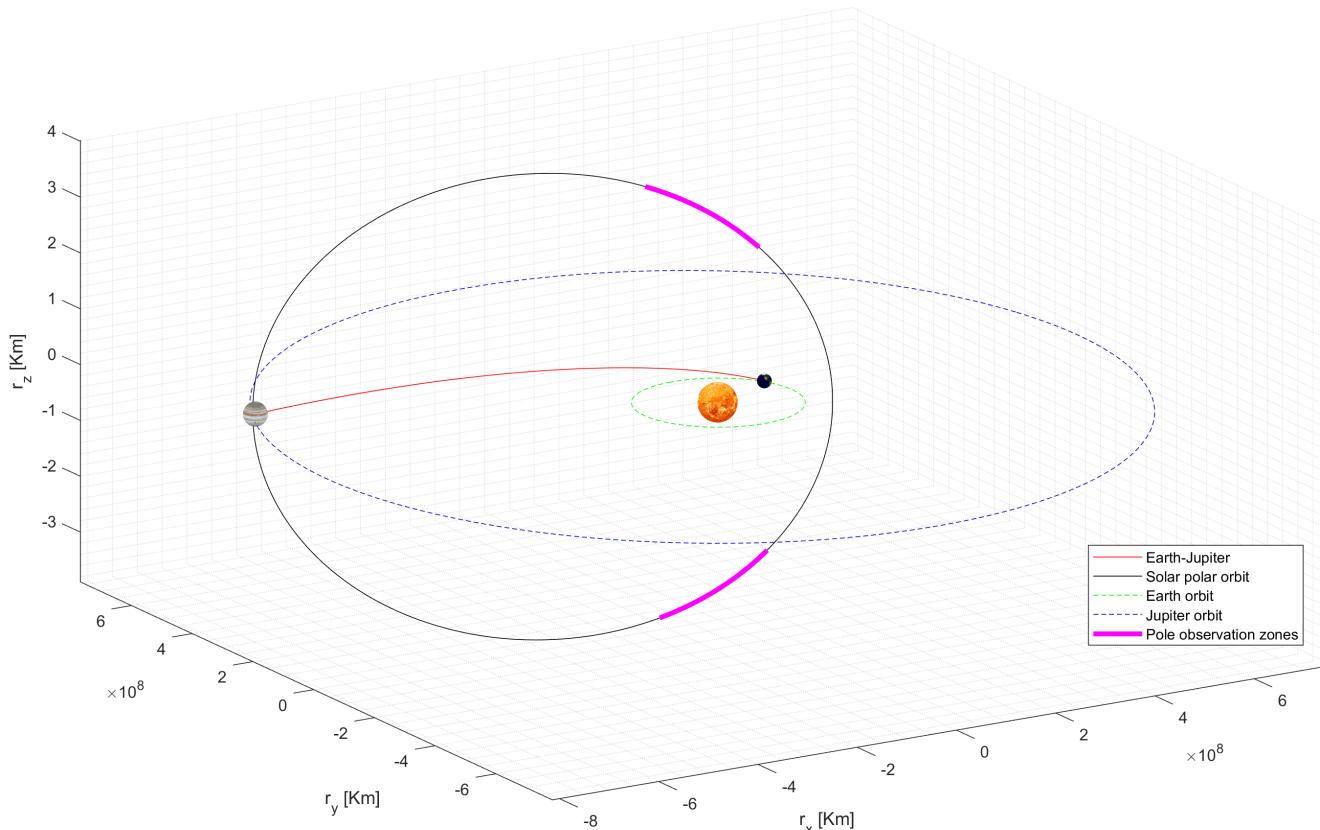


Figure 1.1: Out of Ecliptic orbit

1.2 Mission objectives

The **primary objective** of Ulysses is to determine the three-dimensional characteristics of the heliosphere by in-situ observations. This is achieved by fulfilling more specific objectives that consist of:

- assess the global three-dimensional properties of the interplanetary magnetic field and solar wind
- study the origin of the solar wind by measuring the composition of the solar-wind plasma at different heliographic latitudes
- increase the knowledge of waves, shocks and other discontinuities in solar wind by sampling plasma conditions that are expected to be different from those available near the ecliptic.
- study acceleration of energetic particles in solar flares by observing the X-ray and particle emission from active solar regions
- improve the understanding of galactic cosmic rays by sampling particles over the solar poles, where low-energy cosmic rays may have easier access to the inner solar system than near the ecliptic plane
- advance the knowledge of the neutral components of interstellar gas that enters the heliosphere by measuring its properties as a function of heliographic latitude
- improve the understanding of interplanetary dust by measuring its properties as a function of heliographic latitude

The mission also included **secondary objectives** such as:

- interplanetary physics investigations during the in-ecliptic Earth-Jupiter phase
- study Jupiter's magnetosphere during the flyby
- analyse the composition and estimate the length of comet tails
- look for low-frequency gravitational wave by using the radio communication link
- look for gamma-ray-bursts and, in conjunction with data from other spacecraft, contribute to their identification with known celestial bodies
- detect signals from distant sources in the galaxy

1.3 Functionalities

Considering the objectives previously listed and additional requirements in order to a successful completion it is possible to define the mission's functionalities as it follows:

- the S/C shall reach an OOE orbit
- the S/C shall survive a Jupiter interplanetary transfer and gravity assist
- the S/C shall be able to correctly orient itself as required for communications and measurements
- the S/C shall utilize adequate instruments for the measurements of heliosphere characteristics
- the S/C shall spend at least 150 total days during polar pass (above 70° and below -70° heliographic latitude)

- the S/C shall store/downlink as much data as possible, acquire data almost continuously
- the S/C shall survive at least 5 years at full capability'

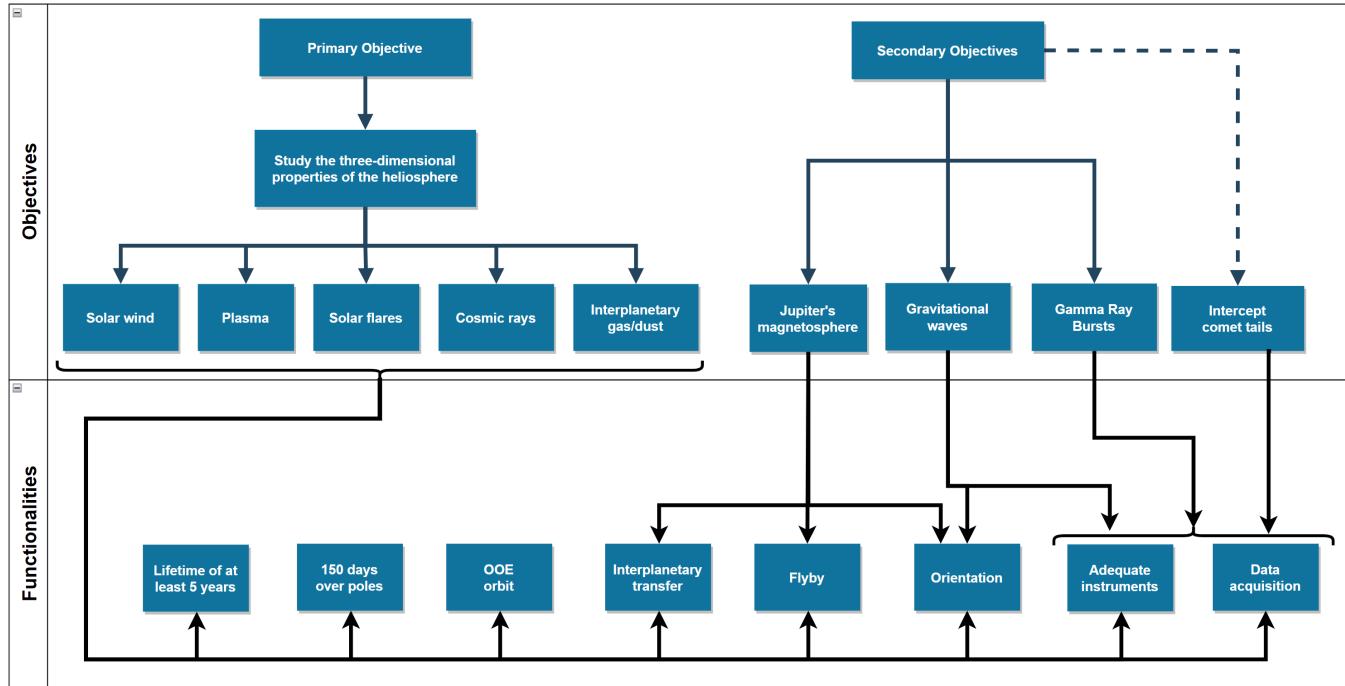


Figure 1.2: Objectives and Functionalities

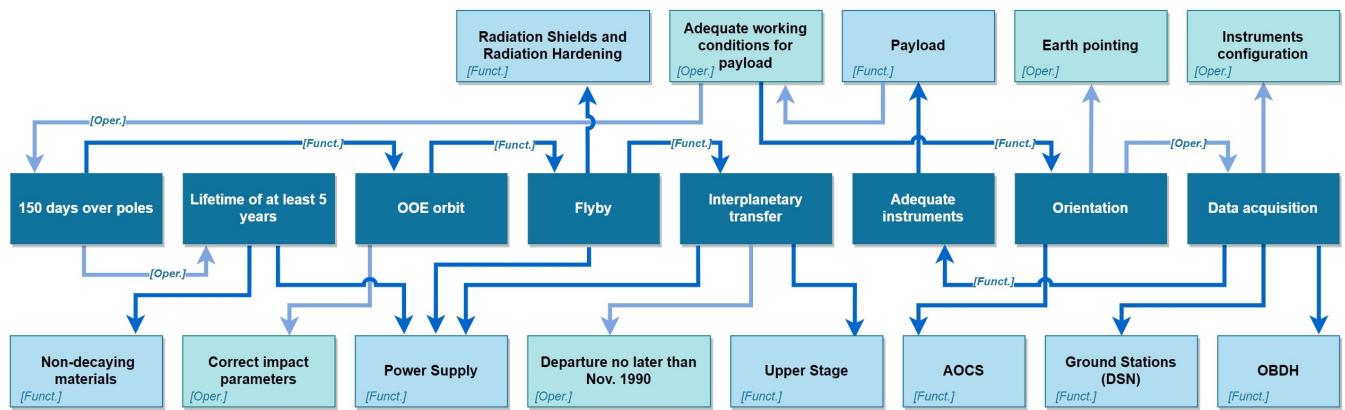


Figure 1.3: Functionalities and Requirements

1.4 Payloads

To carry out measurements required by the mission objectives the spacecraft is provided with several instruments, where each has one or more specific sub-objective which are specified in table 1.1. The position of each instrument inside the spacecraft in launch configuration is illustrated in figure 1.4. Additionally a brief description of the mission's objectives and constraints related to every payload is reported in table 1.1.

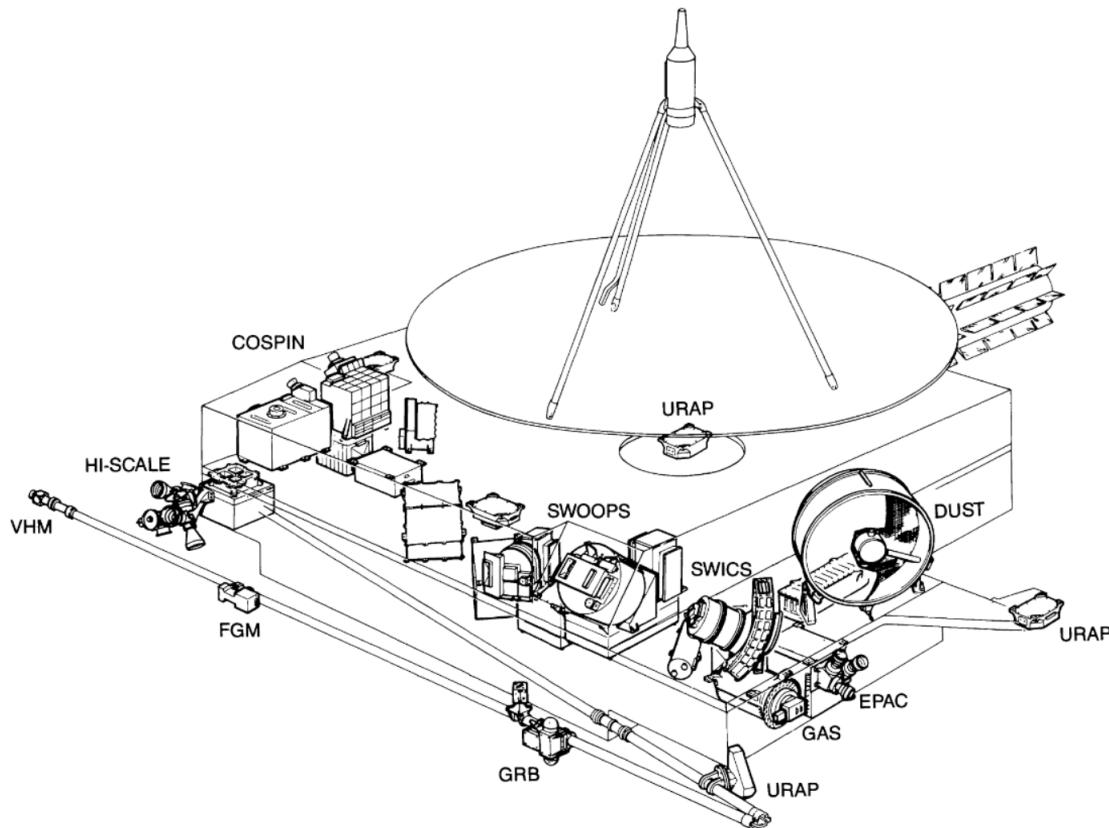


Figure 1.4: Overview of the instruments locations on the Ulysses spacecraft in launch configuration

| Instrument | Related objectives | Constraints |
|------------|--|--|
| COSPIN | <ul style="list-style-type: none"> - Measurements of ions, generally charged particle and cosmic rays to characterize the polar region of the sun and see the differences with the equatorial part. | <ul style="list-style-type: none"> - Shall be isolated from other sources of radiation or particles (e.g. RTG). - Telescopes shall be positioned accordingly to their working angles. - Temperature shall be maintained between -5°C and $+10^{\circ}\text{C}$. |

| | | |
|-----------------|--|--|
| | | - Shall filter bigger particle than the interested ones and not be obstructed. |
| DUST | - Study of interplanetary particles (mass, energy, velocity, density, etc.) in relation to the solar distance. | - Shall be isolated from radiations and charged particles. |
| EPAC/GAS | - Study of the characteristics of interplanetary ions and neutral gas. | - Shall be heated when it reaches very low temperatures. |
| FGM/VHM | <ul style="list-style-type: none">- Determine the dependence of interplanetary magnetic field as a function of solar latitude.- Study the internal dynamics of the solar wind.- Study discontinuities and waves in the interplanetary magnetic field, their formation and propagation and the effect on propagation and acceleration of energetic particles.- Study the structure and dynamics of the dusk region of Jupiter's magnetosphere. | <ul style="list-style-type: none">- Shall be protected from any side penetrating particles.- Shall avoid disturbances generated by the S/C. |
| GRB | <ul style="list-style-type: none">- Detection and study of Solar X-ray emission, cosmic gamma-ray burst and Jovian auroral X-ray radiation. | <ul style="list-style-type: none">- Shall be mounted on the boom in order to minimize interference.- Shall operate in a range of -35°C and -55°C. |

HI-SCALE

- Detection and analysis of electrons and ions in order to better understand solar activities in function of heliolatitude.
 - Study of the possible mechanism of particle acceleration.
 - Shall be mounted in order to obtain nearly all-sky visibility.
-

SWICS

- Study of the solar corona where solar wind is created and accelerated.
 - Study of the causes of variations in the composition of the solar atmosphere.
 - Shall be mounted outside the S/C in order to have access to solar wind.
 - Study of the composition and behaviour of the plasma in the Jovian magnetosphere.
-

SWOOPS

- Investigate and establish bulk flow parameters and internal state conditions of the solar wind as a function of solar latitude.
 - Determine latitudinal variation in solar wind minor ions and in Alfvén waves.
 - Identify local heating mechanisms of solar wind ions and coronal hole temperature.
 - Shall be mounted with its plane of symmetry parallel to the S/C spin axis.
-

URAP

- Determination of the direction, angular size and polarization of radio sources for remote sensing of the heliosphere and the Jovian magnetosphere.
 - Detailed study of local wave phenomena, which determine the transport coefficients of the ambient plasma.
 - The S/C shall have a dedicated deploy system for the antennas.
-
-

| | | |
|------------|--|---|
| GWE | - Evaluate the encounter of low-frequency gravitational waves. | - The S/C must be able to communicate with GSs. |
| SCE | <ul style="list-style-type: none"> - Measure 3D properties of solar corona. - Investigate on plasma bulk velocity. - Measure electron density of the Io plasma torus. | <ul style="list-style-type: none"> - The S/C shall be in solar conjunction. - The S/C must be able to communicate with GSs. |

Table 1.1: Objectives and constraints associated to every single payload

2 Mission analysis, phases and modes

2.1 Phases and modes

The **phases** determined by analyzing the major events occurring during the mission are:

- Launch and parking orbit;
- Interplanetary transfer;
- Flyby;
- OOE orbit.

Consequently, the **modes** identified for each phase are displayed in figure 2.1 and described thoroughly right after it.

- **Launch mode:** The satellite is switched off;
- **Wake up mode:** The satellite is turned on, unfolds the antenna and points towards Earth to establish communications for the first time;
- **TeleCom mode:** The satellite uses part of the power to transmit data to Earth when viable;
- **Idle mode:** The satellite switches off the unnecessary instruments in order to save power;
- **Science mode:** All the instrument are switched on and most of the power is used to acquire and store data.
- **Navigation mode:** The satellite uses part of the power to activate thrusters;
- **Safe mode:** When power safety limits are exceeded non-essential loads are disconnected, rebooted and communication with GS is established.

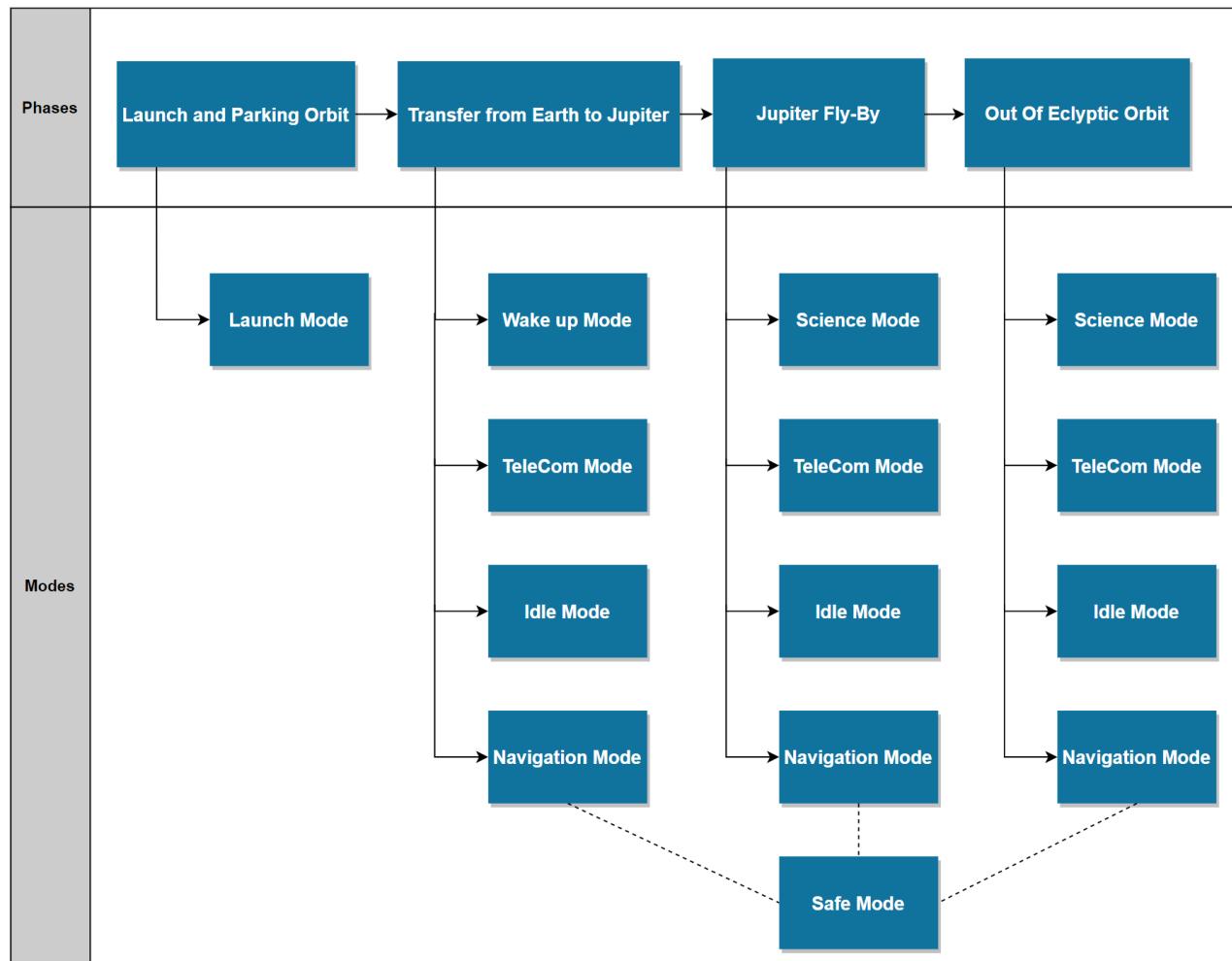


Figure 2.1: Phases and Modes

2.2 ConOps

Once the phases have been identified the ConOps can be defined and are reported in the following schemes in figures 2.2 and 2.3.

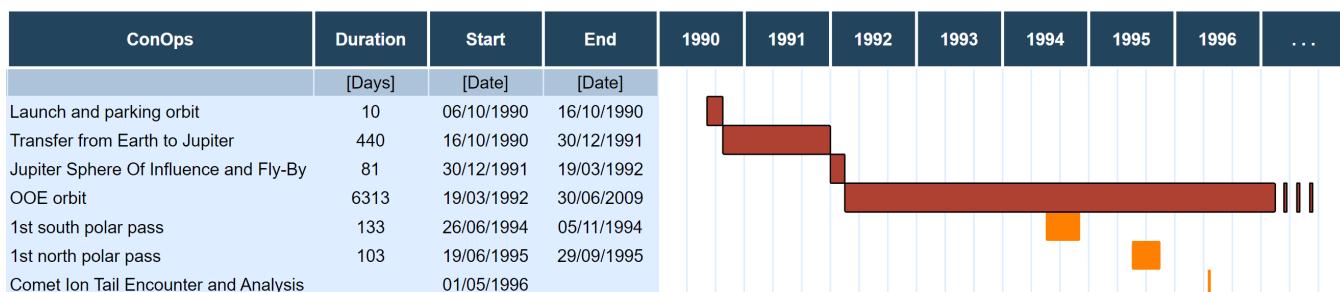


Figure 2.2: ConOps gantt

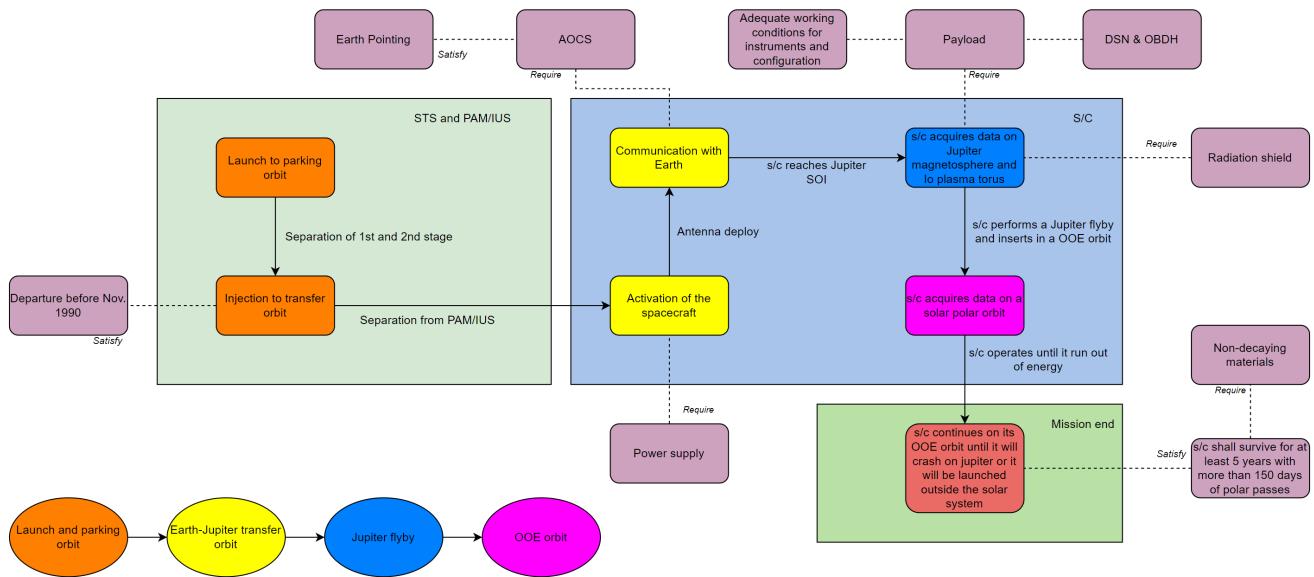


Figure 2.3: ConOps scheme

2.3 Mission analysis

The peculiar functionality of the mission to reach an OOE orbit required to find a way to exit the ecliptic plane. Considering the expensiveness of a change of plane maneuver, especially when the change of inclination is in the order of magnitude of Ulysses', the mission exploited a flyby on Jupiter to gain for free the change of plane needed. Figure A.1 shows Ulysses' entire trajectory, which was extrapolated from its ephemerides available in the Horizon System website from NASA JPL. It also shows the change in inclination due to a close approach to Jupiter after the completion of the second orbit.

2.3.1 Launcher data

Ulysses was launched as the primary payload on the Space Shuttle Discovery (mission STS-41). The launcher comprises of three units: the Orbiter, the External Tank (ET) and two Solid Rocket Boosters (SRBs). The Orbiter, which is responsible for carrying the crew and the payloads, operates three LH₂/LOx liquid rocket engines with the propellant fed by the ET.

Moreover attached to Ulysses there were two upper stages, the Inertial Upper Stage (IUS) and a mission specific Payload Assist Module-S (PAM-S), combined together to send the spacecraft from the parking orbit towards the out-of-ecliptic trajectory.

With the data available on the Space Shuttle Reference Manual [1] it is possible to estimate all the characteristic parameters, listed in table 2.1, needed for the mission analysis. As a consequence the ΔV budget can be summed up into two main components:

- The Space Transportation System's budget, comprised of the stages 1 and 2, which goes from ground to the parking orbit which is approximately 10,3659 km/s.
- The Upper Stage budget, comprised of stages 3, 4 and 5, which enables the spacecraft to be injected into the interplanetary trajectory to Jupiter is approximately 8.4007 km/s

| Stage | Details | ΔV [km/s] | Additional details |
|-------|----------------------|-------------------|-------------------------------------|
| 1 | Orbiter, ET and SRBs | 3.0288 | T+0 s to T+124 s |
| 2 | Orbiter and ET | 1.4312 | T+124 s to T+250 s (Atmospheric) |
| | | 5.9059 | T+250 s to T+480 s (Space) |
| 3 | IUS first stage | 2.3900 | $T_{burn} = 152$ s |
| 4 | IUS second stage | 1.6818 | $T_{burn} = 103.35$ s |
| 5 | PAM-S | 4.3289 | $T_{burn} = 84$ s |

Table 2.1: Stages and related ΔV s

2.3.2 Launch and adjustments in parking orbit

The launch site of Space Shuttle Discovery (STS-41) was in Cape Canaveral, whose coordinates are $28^\circ 28'$ N $80^\circ 32'$ W. Considering the launch site, the minimum attainable orbital inclination is 28.46° . Moreover Earth has an axial tilt with respect to the ecliptic plane of 23.43° as of January 1st 2021.

Consequently, to do an efficient interplanetary transfer to Jupiter the inclination of the parking orbit has to be 25.39° , which is the sum between the axial tilt of Earth and the inclination of the transfer orbit both with respect to the ecliptic plane.

One possibility considered is to exploit the asphericity of Earth, in particular the J_2 effect which is the most dominant for Earth's gravitational field, while in the parking orbit to change the inclination to the desired one. Effectively the obtained variation in 10 days is 0.0356° which is way lower than the needed one. To do this adjustment of inclination we can do a simple change of plane maneuver which will result in a ΔV , if done at the ascending node, equal to 0.4192 km/s which is feasible with respect to the ΔV budget available. Figure A.2 also shows the injection into the interplanetary transfer towards Jupiter that will be discussed in the next section.

2.3.3 Injection in interplanetary transfer

After the insertion into the parking orbit the spacecraft is ready to begin its journey to the interplanetary transfer by giving an impulse to exit Earth's SOI. The orbital parameters and the trajectory of the interplanetary transfer are displayed respectively in equation 2.1 and figure A.3.

$$\text{OP}_{\text{transfer leg}} = \begin{Bmatrix} a \\ e \\ i \\ \Omega \\ \omega \end{Bmatrix} = \begin{Bmatrix} 1345106000 \text{ km} \\ 0.889166 \\ 1.990719^\circ \\ 12.85909^\circ \\ 7.72595^\circ \end{Bmatrix} \quad (2.1)$$

With these data available it is possible to calculate the ΔV_{inj} necessary to inject Ulysses in the interplanetary trajectory and is, using the patched conics approximation, equal to 8.0278 km/s, which is compatible with the budget available from the upper stages of the mission.

Additionally the launch date is justified by the pork-chop plot for an Earth-Jupiter transfer, visible in figure

2.4, where it is possible to see that the selected dates for departure and the gravity assist are coherent with a minimization of the impulse needed for injection. The actual minimum was not chosen because it would imply an additional year of interplanetary transfer without scientific investigation on the main objectives and consequently the need for more radioactive material for the RTG.

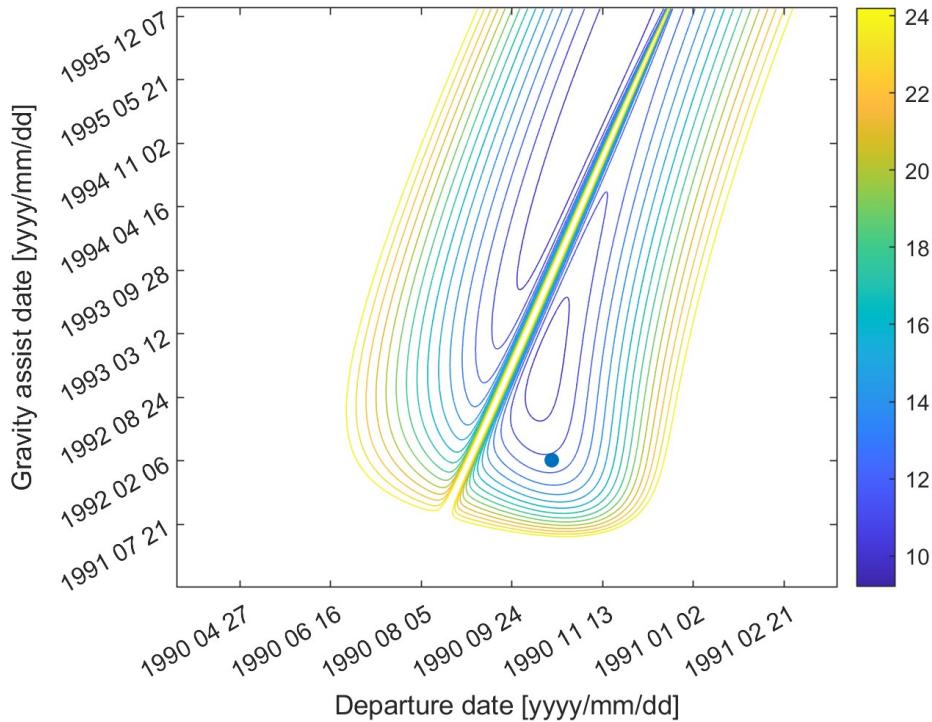


Figure 2.4: Pork-chop plot for the Earth-Jupiter arc

2.3.4 Flyby of Jupiter

As previously mentioned the flyby on Jupiter was done in order to obtain a free ΔV that would be impossible to achieve by using any propulsion system, especially for the ones on board of an interplanetary mission. More specifically ΔV obtained with this maneuver is 16.9 km/s.

The orbital parameters, obtained indirectly using Ulysses' ephemerides in the Jovian reference frame, and the flyby trajectory are displayed respectively in equation 2.1 and figure A.4. It is important to underline that the inclination of the flyby was chosen to obtain the necessary ΔV but also to avoid the radiation belt inside Jupiter's magnetosphere which would cause damage to the payloads. Nevertheless the opportunity to study Jupiter's magnetosphere was exploited to the greatest extent. Ulysses was able to produce a wealth of new information relating to the Jovian magnetosphere, also by penetrating Io's plasma torus.

In order to perform the unpowered flyby on Jupiter that would place Ulysses in the correct final OOE orbit, the spacecraft needed some corrective maneuvers. Unfortunately no data about the entity and the time of these corrections is available. On the other hand they can be modeled using the patched conics approximation as a powered flyby with an impulse given at the pericenter of the inbound hyperbola. The value of this impulse is found by subtracting the pericenter velocity of the outbound hyperbola with the inbound one. The first one is found by considering the value of the needed velocity of the outbound hyperbola in order to reach the final desired orbit. By using this approximation the impulse needed for the corrections turns out to be 0.1327 km/s, which is feasible but surely overestimated.

2.3.5 OOE orbit

After the flyby of Jupiter the final orbit of Ulysses is shown in figure 1.1 and subsequently its orbital parameters displayed in equation 2.2.

Moreover in figure 1.1 is also highlighted the moments where the spacecraft has an altitude with respect to the Solar equator that is higher than $+70^\circ$ and lower than -70° . The total time passed by Ulysses in the polar regions of the Sun in one orbit sums up to approximately 220 days, which fulfills the functionality to spend at least 150 days in these regions.

$$\text{OP}_{\text{OOE}} = \begin{Bmatrix} a \\ e \\ i \\ \Omega \\ \omega \end{Bmatrix} = \begin{Bmatrix} 504594094 \text{ km} \\ 0.60306 \\ 79.12801^\circ \\ 337.4814^\circ \\ 358.8862^\circ \end{Bmatrix} \quad (2.2)$$

2.4 Mission Analysis design effects

Due to high inclination of the OOE orbit with respect to the ecliptic plane it is necessary to evaluate the ground tracks defined by the spacecraft during the solar polar passes in order to understand the coverage needed by the ground station on Earth.

The ground track, displayed in figure 2.5, are traced using the ephemerides downloaded from NASA/JPL Horizon System centred on Earth during South and North polar passes with a time step of 1 hour. As

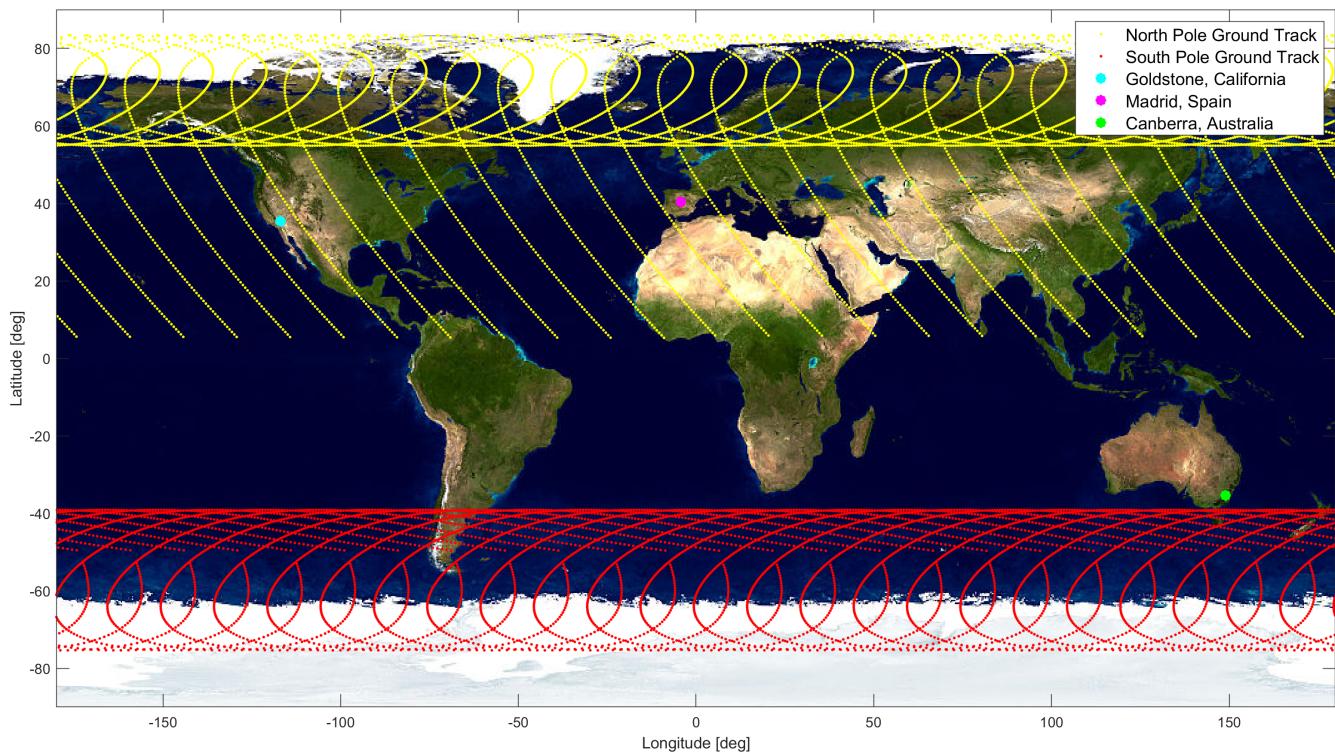


Figure 2.5: Ground track during a Polar passes

it is possible to see, during the South solar passes latitudes vary from -40 to -75 degrees and from $+5$ to $+83$ degrees during North solar passes. The values obtained explain why Ulysses mission must rely on the three ground station that compose the Deep Space Network (DSN), situated in:

- Canberra, Australia

- Goldstone, California
- Madrid, Spain

The DSN Ground Station in Canberra is able to provide nearly continuous coverage of the S/C during South polar passes while the ones in Madrid and Goldstone are responsible of the S/C during North Polar passes.

2.5 Possible alternatives for the mission

2.5.1 Simple change of plane maneuver

As previously stated in Ulysses' mission design the simple change of plane maneuver was avoided since it comes to a very high cost. The quantification of this cost for the most generic change of plane maneuver can be easily done by using equation 2.3. Considering the parameters of both the transfer and the OOE orbits this ΔV can be easily calculated as:

$$\Delta V = \sqrt{V_1^2 + V_2^2 - 2V_1V_2(\cos\Delta\gamma - \cos\gamma_1\cos\gamma_2(1 - \cos\delta))} \approx 16.7 \div 17.3 \text{ km/s} \quad (2.3)$$

where the subscripts 1 and 2 respectively represent quantities before and after the change of plane. This result is very high compared to the free change of plane obtained by exploiting Jupiter's gravity.

2.5.2 Flyby alternatives

Another possibility could have been a flyby on Mars instead of Jupiter in order to acquire the desired final orbit. In a similar manner to what has been said about the Earth-Jupiter arc also for the Earth-Mars' one the dates of departure and flyby correspond to a minimization of the ΔV required for the injection, as can be seen in figure A.5. In order to obtain the required ΔV for the change of plane, Ulysses would need to have a pericenter radius of the hyperbolic flyby trajectory of 57 km, which is lower than Mars' radius, resulting in an impossible maneuver (see figure A.6).

To a similar extent, the same things can be said about a flyby on Venus. Other possibilities (e.g. exploiting Saturn's gravitational field for the desired change of plane) haven't been considered since they would require additional flybys to reach it and it would elongate enormously the TOF.

2.6 Environmental analysis

The environmental analysis can be schematically divided into three main phases:

- Transfer from Earth to Jupiter:
- Jupiter's flyby:
- OOE orbit:

In all the phases of the mission solar radiation pressure shall be considered. Usually the values are small (e.g. at 1 AU is approximately $4.5 \mu\text{Pa}$) but considering the long journey of the spacecraft the disturbance will affect its trajectory in a non-negligible way. This effect shall be controlled by the spacecraft's control system accordingly.

Moreover, during Jupiter's flyby the effect of radiations shall be considered. The action of the Jovian magnetosphere traps and accelerates particles, producing intense belts of radiation, similar to Earth's Van Allen belts, but thousands of times stronger. Previous missions such as Mariner 10 and Pioneer 11 demonstrated that spacecraft could survive in high radiation areas. They also taught us that materials needed to be radiation hardened, otherwise we would have irreversible damage to the spacecraft electronics and payloads.

Another factor that needs to be examined during the flyby, and in general during the time the S/C is inside Jupiter's magnetosphere, is the presence of intense magnetic fields. These can cause disturbances on the instrumentation and unwanted torques on the S/C. The problem can be addressed by using magnetic field shields, compatibly with the needs of instrumentation, and with an appropriate control system.

Furthermore, the main environmental criticality during the OOE orbit, also present in the transfer leg to Jupiter, is temperature gradients. The vast difference in distance between apocenter and pericenter of the orbit, respectively 5.4 AU and 1.3 AU, make temperature gradients non-negligible. More specifically, using radiative equilibrium, temperatures range from roughly -111° C at the apocenter to $+55^{\circ}$ C in the closest point to the Sun. Active thermal control solutions (e.g. dissipators) can be applied to solve this problem.

3 Propulsion s/s

3.1 Subsystem description

Ulysses' propulsion system comprises only of a secondary propulsion unit which serves its Attitude and Orbit Control System. More in particular, it uses 2 series of 4 catalytic thrusters mounted on +X and -X wing that allow control of the spin rate and along axis Z. Thrusters can also be controlled by telecommand; thruster firing phase, on-time, and number of pulses can be calculated on the ground and loaded directly to the AOCS. Additional informations about the thrusters are shown in table 3.1.

More in detail, thrust is provided by catalytic decomposition of high purity anhydrous hydrazine (N_2H_4) stored inside a spherical tank placed as close as possible to the spacecraft's centre of gravity.

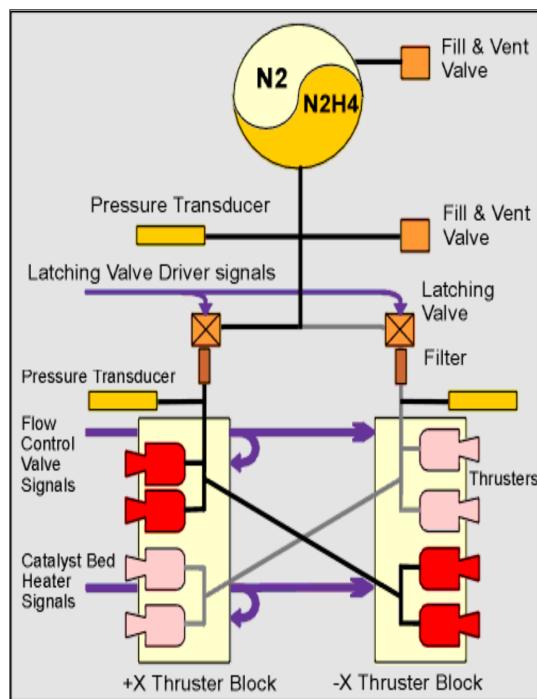


Figure 3.1: Architecture propulsion system

almost linearly since the thrusters were used only for corrections manoeuvres (e.g. Earth pointing in order to transmit and receive data).

Analyzing the propulsion system's architecture (displayed in figure 3.1) it is possible to observe that the two pipes' branches feed both the two block of thrusters. This redundancy is done so that, in case of failure of one branch, the spacecraft does not completely lose control of one of its thruster block.

The position was chosen in order to minimize the excursion of its centre of gravity due to the variation of the level of hydrazine during the lifetime of the spacecraft, on the other hand, the shape was designed to guarantee an optimal structural-wise stress concentration while storing pressurized hydrazine.

Table A.3 reports the data about propellant mass stored and temperature of the tank during the lifetime of the spacecraft. At the beginning of the mission, the tank was filled with 33.491 kg of anhydrous hydrazine at the pressure of 22 bar and a temperature of 20° C, the total volume of the tank was 0.04491 cubic meters.

Furthermore, the tank had a propellant mass drop from 33.491 kg to 15.473 kg in the time span of a month. The pressure in the tank changed accordingly from 22 bar to 8.83 bar. This was due to a corrective manoeuvre that stabilized the spacecraft after the injection in the interplanetary transfer towards Jupiter and then increased further its velocity. The propellant used in this manoeuvre is 18.018 kg, which is about 53.80% of the total propellant mass and corresponds to a ΔV of about 0.1 km/s. This value is in the same order of magnitude of the one obtained in the Mission Analysis. The remaining propellant, which was used for the rest of the mission, decreased only for corrections manoeuvres (e.g. Earth pointing in order to transmit and receive data).

| | |
|---------------------|-----------|
| Model | CHT2 |
| Thrust | 2 N |
| Power | 2.2 kW |
| Propellant | Hydrazine |
| Chamber Pressure | 22 bar |
| Weight | 200 g |
| Length | 123 mm |
| Nozzle Diameter | 8.66 mm |
| Equivalent Speed | 2230 m/s |
| Minimum impulse bit | 0.01 N·s |

Table 3.1: Ulysses' thrusters specifications

3.2 Propellant selection

Hydrazine was chosen for its simplicity, reliability and efficiency. One of the main advantages of using a mono-propellant, instead of a bi-propellant, is that the propulsion system is lighter and smaller due to the need of only one tank and less valves needed in general. Moreover, it grants restartability and throattability which is ideal for attitude control maneuvers.

On the other hand, the use of hydrazine introduces two pivotal aspects that need to be taken into account when designing propulsion subsystem:

- Gas production due to dissociation
- Freezing point

Additional details are illustrated in the following paragraphs.

3.2.1 Gas production due to dissociation

One of the major concerns in storing hydrazine is the gas production due to its dissociation when in contact with materials or impurities derived from the manufacturing process. This behaviour of the propellant required the choice of a Titanium alloy (Ti-6Al-4V for Ulysses) for the tank and pipes surfaces in contact with hydrazine since it is particularly compatible with hydrazine. Furthermore, the spherical shape combined with the nominal spin rate of the spacecraft ensured that gas remained confined in the central part of the tank. Unfortunately, as the tank became depleted of hydrazine, more of the gases resulted from the dissociation entered the pipe system resulting in ‘gassy’ pulses of thrusters. This required additional correctional pulses in order to obtain the desired configuration.

3.2.2 Freezing point

Another criticality with hydrazine is that its freezing point is at $+2^{\circ}\text{C}$. As shown in the Mission Analysis from a rough estimation, the temperature of the S/C in the OOE orbit ranges from a maximum of $+55^{\circ}\text{C}$ at the pericenter to -111°C at the apocenter. Consequently, the spacecraft needs to have a Thermal Control subsystem in order to keep the tank in a limited range of temperatures, which would otherwise lead to a catastrophic failure.

The temperature of the tank at the start of the mission was 20°C , which also minimized the gas production derived from dissociation. This temperature was maintained constant thanks to the Radioisotope Thermoelectric Generator (RTG) present on board which produced electric energy from the decay of PuO_2 .

Being the initial power output of the RTG 285 W keeping the temperature of the tank around 20°C was completely feasible. Moreover, in the early phase of the mission, especially during perihelion, the system needed the intervention of the Internal Power Dumping system in order to dissipate locally heat radiated by larger power-consuming units. Throughout the years of the mission the RTG decreased its power output almost linearly which implied that the storage of hydrazine above freezing condition would become always more challenging, to the point where at the beginning of the third orbit around the Sun the tank was operating only few degrees above the freezing point of hydrazine.

3.3 Mission analysis ΔV s required

The mission analysis highlighted the need for two main ΔV s. The first one related to the corrections needed in order to perform Jupiter's gravity assist and the second one for attitude control. Further details are presented in table 3.2.

| Type | Value | Related margin |
|----------------------|---------------|----------------|
| Flyby corrections | 0.1327 km/s | 10 % |
| Attitude corrections | 0.008 m/s/day | 100 % |

Table 3.2: ΔV s from the mission analysis

From this data the propulsion subsystem is sized based on the total ΔV needed for these maneuvers, considering the time-span of the mission being 6 years.

3.4 Sizing of the tank

From the ΔV s required for the mission and the propellant selection it is possible to size the tank where the hydrazine is stored. From the total ΔV needed for the mission, which sums up to 0.181 km/s considering the relative margins, the propellant mass needed can be easily computed from Tsiolkovsky equation. Consequently all the other parameters can be calculated as a cascade, always considering their related margins. The quantities of interest are computed, reported and compared to the real ones in table

| Quantity | Related margin | Computed value (including margin) | Real value |
|------------|----------------|--------------------------------------|-----------------------|
| m_{prop} | 2.5% | 34.83 kg | 33.5 kg |
| V_{tank} | 10 % | 0.0503 m ³ | 0.0449 m ³ |
| m_{gas} | 20 % | 0.3812 kg | - |
| r_{tank} | - | 0.2289 m | 0.22 m |
| t_{tank} | - | 0.549 mm | - |
| m_{tank} | - | 1.603 kg | 7.0 kg |

Table 3.3: Sizing quantities of the Propulsion Subsystem

It is important to highlight that the value computed for t_{tank} , and consequently m_{tank} , is the minimum value for the tank to withstand its internal pressure.

Additionally, the value obtained for the tank mass is computed considering a sphere subjected only to the

internal pressure of the propellant, while in a real sizing also structural loads due to high accelerations (e.g. launch, injection manoeuvre) must be considered. Moreover, the mass obtained refers only to the spherical shell without taking into account the mass of all the other components such as mounting system, pressure and temperature transducers and the ethylene propylene membrane.

3.5 Inertia moments and barycentre evaluation

Adopting a simplified model of Ulysses spacecraft, the geometrical centre, the barycentre and the principal moments of inertia are computed. Both centre of mass and moments of inertia change over time according to propellant mass variation showing an almost linear trend with a small excursion from the initial value.

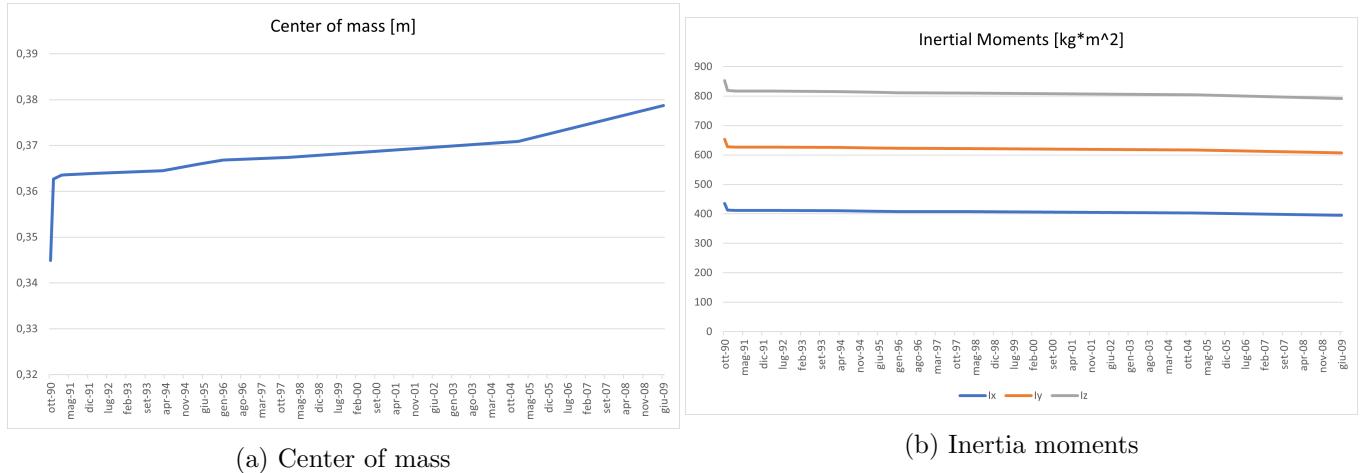


Figure 3.2: Center of mass and inertia moments variation with time cause by depletion of the propellant

The position of the centre of mass is defined with respect to the geometrical centre of the spacecraft in the direction of the RTG, which represent the more massive element outside the central part of the spacecraft. The total displacement is about 2 cm over the entire lifetime of the mission, validating the choice of placing the tank centred in the barycentre.

3.6 Environmental effects

3.6.1 Temperature

Considering the relatively low point of freezing of hydrazine the Thermal Control and Electrical Power substystems must be sized accordingly, also considering the fact that due to the high eccentricity of the OOE orbit the spacecraft experiences high non-negligible variations of its temperature.

3.6.2 Zero-gravity effects

Zero-g environments cause fluids to behave differently from we are used to. In fact, a phenomenology observed in these environments is related to the creation of bubbles which can cause problems in directing the propellant towards the outlet. From an operational point of view, a basic requirement for any propulsion system using liquid propellant is the assurance of the immediate availability of a single-phase propellant at the tank outlet in order to have a proper engine ignition. [2]

Generally three solutions can be found:

- Micro-accelerations: Using an acceleration device that temporarily applies an acceleration field in order to cancel out the zero-g effects

- Negative expulsion devices: They exploit the surface tension of a liquid in order to reduce the undesired effect.
- Positive expulsion devices: They use physical barriers between the propellant and pressurizing gas. It's important to note how these surfaces tend to be flexible so that they can also prevent sloshing problems by adjusting on the levels of the decreasing propellant and pressurizing gas.

In the case of Ulysses, the low spin rate of 5 rpm, coupled with concerns associated to the interaction between propellant sloshing and the spacecraft's dynamics [3], led to the decision to adopt a positive expulsion diaphragm in order to separate the propellant from the pressurizing gas.

3.7 Propulsion system mass and power consumption

The mass and the power consumption have been estimated from literature, past mission and data from similar component available on market. Table 4.8 briefly lists the values related to each component of the PS.

| Component | N° of components | Mass [kg] | Mean Power[W] |
|---------------------|------------------|--------------|---------------|
| Propellant tank | 1 | < 7 | - |
| Thruster | 8 | 0.2 | < 6 |
| Pressure transducer | 3 | 0.6 | 0.01 |
| Latching valve | 2 | 0.7 | 6 |
| Flow control valve | 2 | 0.15 | 5.5 |
| Fill and vent valve | 2 | 0.15 | 5.5 |
| Filter | 2 | 0.35 | - |
| Total | 20 | 12.75 | 82.03 |

Table 3.4: Estimated mass and power consumption of each component

4 Tracking, Telemetry and Telecontrol s/s

4.1 Subsystem description

The communication subsystem provides capabilities for telemetry, ranging, telecommand and radio science. The operational details are resumed in table 4.1. The subsystem includes two redundant transponders,

| Operational band | Frequency | Used for |
|------------------|-----------|---------------------|
| X-band | 8.4 GHz | downlink and uplink |
| S-band | 2.4 GHz | uplink |

Table 4.1: Communication subsystem summary

two redundant 20 W X-band Travelling-Wave-Tube Amplifiers, a TWTA interface unit and a S-band Radio-Frequency Distribution Unit. In the figures A.7a and A.7b a schematics of the TTMTC structure is presented.

The High Gain Antenna which is the primary element for communication link is a 1.65 m parabolic dish made of honeycomb reinforced carbon fibres. Furthermore, a Low Gain Antenna (LGA-F) is also present and mounted on three support struts of the HGA and provides hemispherical coverage for the S-band downlink when, in the early times of the mission, the spacecraft was not pointed toward Earth. Moreover, another Low Gain Antenna (LGA-R) is mounted on opposite side of the spacecraft with respect to the LGA-F. It was used only when HGA and LGA-F was not pointing Earth. The LGA-R wasn't routinely used after the first phases of the mission; however it could be used as a backup receive antenna in the highly unlikely event that uplink was not possible through the HGA or LGA-F.

4.2 Ground Stations description and visibility

As previously stated in the Mission Analysis design effects and consequently in figure 2.5, the GSs of the DSN that Ulysses mainly relies on are the ones in Canberra, Australia; Goldstone, California; Madrid, Spain. Furthermore, the DSN GS in Canberra is able to provide nearly continuous coverage of the S/C during South Polar passes while the ones in Madrid and Goldstone are responsible of the S/C during North Polar passes. In addition, ESA's deep-space antenna DSA 1 in New Norcia (Australia), the ESTRACK station in Kourou and non-DSN NASA stations are used, as well as other agencies' stations including the German Aerospace Center's Weilheim and Chile's Santiago stations.

4.2.1 Visibility

The DSN ground stations are approximately 120° degrees apart around Earth in order to cover almost the entire globe of Earth; nonetheless, as shown in figure 2.5, in the southern part of South America and part of the Atlantic Ocean a coverage gap is present. On the other hand, it has to be noted that the percentage of ground covered from the DSN increases with the distance of the spacecraft from Earth surface following an approximated logarithmic law [4]:

$$DSN\%_{\text{coverage}} = 99.087 + \frac{0.391 + 0.1215R}{9.21R} \ln(R - 1) \quad (4.1)$$

where R is the distance of the spacecraft with respect to Earth in millions of kilometres.

During its heliocentric orbit Ulysses' distance from Earth varies greatly, an average value for the DSN coverage is 99.16 %. Ulysses is tracked 8 hours per day by a 34 m antenna of the Deep Space Network, while it is tracked almost continuously during Sun polar passes by 34 or 70 m antenna.

4.3 Telemetry and tracking

The telemetry data is stored in two redundant tape recorders with a capacity of 45.8 Mbit each, while the data rates are reported in the table 4.2. On the other hand, Earth pointing is achieved by Ulysses

| Mode | Data rate |
|---------------|------------|
| Tracking mode | 1024 bit/s |
| Storage mode | 512 bit/s |

Table 4.2: Tracking data rates

exploiting the CONSCAN Processor which takes Automatic Gain Control signals from the receivers in

the TT&C subsystem and uses them to determine the pointing error between the Earth direction and the HGA boresight, and to determine the direction of this off pointing. This information is then used to generate thruster pulses to move the spacecraft spin axis in the correct direction to keep the spacecraft Earth-tracking. At this purpose, the HGA axis is slightly shifted with respect to the spin axis. This offset feed combined with the spacecraft spin introduced an apparent oscillation to a radio signal transmitted from Earth when received on board the spacecraft. The amplitude and phase of this oscillation were proportional to the orientation of the spin axis relative to the Earth direction.

4.4 Sizing of the TTMTC

The purpose of the sizing is to do a preliminary analysis on the possible diameters of the different antennas that are on board of Ulysses, varying the signal to noise ratio in order to guarantee an acceptable quality for the communications. As previously mentioned, in order to maintain contact with Earth the S/C relies on the DSN's ground stations, mainly the 34 and 70 m antennas, and it uses two bands, X-band and S-band, depending on the phase of the mission and type of communication.

4.4.1 X-band

4.4.1.1 High Gain Antenna The HGA is the only antenna that is on-board of Ulysses that operates in the X-band. More specifically, it's a parabolic dish that operates mainly as a primary communications link for telemetry. The following parameters reported in table 4.3 are the ones assumed in order to size the antenna. With these values assumed it is possible to obtain the sized quantities that are reported in table 4.4.

| P_{tx} | bit-rate | f | B | G_{DSN} (70m) | G_{DSN} (34m) | T_{noise} | BER | $\frac{E_B}{N_0} _{req}$ |
|----------|------------|-----------|---------|--------------------|--------------------|-------------|-----------|--------------------------|
| 20 W | 1024 bit/s | 8.408 GHz | 125 kHz | 74.25 dB | 67.98 dB | 13 K | 10^{-7} | 12 dB |

Table 4.3: Assumed parameters for the sizing of the HGA

| Quantity | Margin | DSN 70m | DSN 34m | Real values |
|------------------------------|--------|---------------|---------------|----------------------------|
| Carrier signal to noise [dB] | - | 40 ÷ 60 | 40 ÷ 60 | 53.15 (34m) 58.84 (70m) |
| Antenna Diameter [m] | - | 0.18 ÷ 1.88 | 0.39 ÷ 3.88 | 1.65 |
| $G_{antenna}$ [dB] | - | 21.80 ÷ 41.80 | 28.07 ÷ 48.07 | 40.63 |
| E_b/N_0 [dB] | - 3 dB | 64.70 ÷ 84.70 | 64.70 ÷ 84.70 | 77.27 (34m) 83.54 (70m) |
| EIRP [dB] | - | 33.81 ÷ 53.81 | 40.08 ÷ 60.08 | 52.66 |

Table 4.4: Sized values for the HGA in X-band

As it is possible to see from the results, the diameter of the High Gain Antenna can be chosen between 0.39 m and 1.88 m, since also smaller ground station antennas has been occasionally used the lower bound should be increased further. The upper bound is related to the total mass of the structure which grows exponentially increasing the diameter of the HGA. Another major constraint identified is the space available during the launch phase.

4.4.2 S-band

4.4.2.1 Low Gain Antennas Ulysses is also equipped with two LGAs that operate in the S-band. These are much smaller with respect to the HGA and are used only in the early phases of the mission or in case of problems with the primary link system. They communicate only in the S-band which is primarily used for ranging and radio-science.

As seen for the HGA antenna in the X-band, the parameters adopted for the sizing of the LGAs are reported in table 4.5. Consequently the sized quantities can be computed and are reported in table 4.6.

| P_{tx} | bit-rate | f | B | G_{DSN} (70m) | G_{DSN} (34m) | T_{noise} | BER | $\frac{E_b}{N_0} _{req}$ |
|----------|--------------|-----------|--------|--------------------|--------------------|-------------|-----------|--------------------------|
| 5 W | 15.625 bit/s | 2.293 GHz | 35 kHz | 62.97 dB | 56.70 dB | 13 K | 10^{-5} | 4.4 dB |

Table 4.5: Assumed parameters for the sizing of the LGA

| Quantity | Margin | DSN 70m | DSN 34m | Real values |
|--------------------------------------|--------|--------------------|--------------------|----------------------------|
| Carrier signal to noise [dB] | - | 10 \div 20 | 10 \div 20 | 10.46 (34m) 16.73 (70m) |
| Antenna Diameter [m] | - | 0.023 \div 0.073 | 0.047 \div 0.15 | 0.05 |
| $G_{antenna}$ [dB] | - | -7.73 \div 2.27 | -1.46 \div 8.54 | -1 |
| E_b/N_0 [dB] | - 3 dB | 47.34 \div 57.34 | 47.34 \div 57.34 | 47.80 (34m) 54.07 (70m) |
| EIRP [dB] | - | -1.74 \div 8.26 | 4.53 \div 14.53 | 4.99 |

Table 4.6: Sized values for the LGA in S-band

4.4.2.2 High Gain Antenna Additionally, the HGA also operates in the S-band for receiving purposes. Following the same procedure as for the X-band starting from the values in table 4.3 we obtain the sized values for the HGA in the S-band, reported in table 4.7.

| Quantity | Margin | DSN 70m | DSN 34m | Real Data |
|-------------------------------------|--------|---------------|---------------|----------------------------|
| Carrier signal to noise [dB] | - | 40 ÷ 50 | 40 ÷ 50 | 40.83 (34m) 47.09 (70m) |
| Antenna Diameter [m] | - | 0.73 ÷ 2.30 | 1.50 ÷ 4.74 | 1.65 |
| Antenna Gain [dB] | - | 22.27 ÷ 32.27 | 28.54 ÷ 38.54 | 29.37 |
| Eb/N0 [dB] | - 3 dB | 77.34 ÷ 87.34 | 77.34 ÷ 87.34 | 78.17 (34m) 84.44 (70m) |
| EIRP [dB] | - | 28.26 ÷ 38.26 | 34.53 ÷ 44.53 | 35.36 |

Table 4.7: Sized values for the HGA in X-band

4.5 TTMTTC mass and power consumption

From the architecture and the knowledge of the TTMTTC subsystem it is possible to estimate the power consumption of the whole subsystem. Table 3.4 briefly lists the values related to each component of the subsystem.

| Component | N° of components | Mass [kg] | Mean Power [W] |
|--------------------|------------------|-----------|----------------|
| Transmitter X-Band | 2 | 0.3 | 20 |
| Transmitter S-Band | 2 | 0.2 | 5 |
| TWTA X-Band | 2 | 1 | 20 |
| Receiver | 2 | 0.5 | 4 |
| RFDU | 2 | <1 | 1 |
| Data Storage Unit | 2 | <1 | 8 |
| HGA | 1 | <6 | - |
| LGA | 2 | <1 | - |
| Total | 15 | 16 | 116 |

Table 4.8: Estimated mass and power consumption of each TTMTTC s/s component

4.6 Environmental effects

4.6.1 Conjunctions and Oppositions

Telecommunication performances can be affected by the conditions in which the spacecraft is operating, for example, during solar conjunctions, the radio path between the Earth and the spacecraft traverses the Sun's coronal region. As a result, downlink is usually severely degraded because the radio frequency noise from the Sun is so overwhelming that telemetry arriving at the ground station is corrupted to the extent that the error correction coding is becomes useless.

In general, the telecommand has a greater immunity from this effect due to its low bit rate (nominally 15.625 bit/s) compared to the telemetry bit rates. Nevertheless, the effect on the uplink is not insignificant because the on-board CONSCAN measurements become noisier. This results in greater uncertainties in the attitude determination. [5].

During these periods the CONJ manoeuvre strategy has been successfully adopted. The CONJ manoeuvres are open-loop slews executed by the on-board CONJ program based on a fixed set of thrusters firing parameters, repetition count and execution interval which are uplinked from the ground. Typically, the CONJ parameters are set to produce a sequence of slews which take the spacecraft attitude around the Sun instead of directly following the Earth path past the Sun. [5]

The conjunction geometry can impact spacecraft operations since it may compromise the capability to command or monitor the spacecraft. So, for conjunctions where the alignment is good, all critical operations for a protracted period are loaded on-board the Ulysses spacecraft well in advance.

In addition some other special operations may be required as well as:

- Switching off the tape recorders to use the power for the S-band transmitter
- S-Band transmitter switch on for Radio-Science, and a corresponding thermal reconfiguration
- Suspending the routine commands to the Ulysses scientific instruments

Figure 4.1 shows the moments where conjunctions and oppositions occur. As can be seen from tables A.4 and A.5, during conjunctions the Radio-Science Solar Corona sounding experiment is performed, using Doppler and ranging data to determine the density, velocity and the dynamics of solar corona. Radio-Science experiments have not been performed during all of Ulysses' Conjunctions since the spacecraft-Sun-Earth alignment has not always been good enough. Also, during the Second Solar Orbit, power constraints have limited the use of the S-band transmitter. On the other hand, during oppositions, there is minimal solar interference to the radio signals travelling between the Earth and the spacecraft. It is therefore a good opportunity to try to detect gravitational waves. Second Opposition in February 1992 provided the best geometric conditions for the GWE. First Opposition was therefore used as a period to test the radio science techniques. No GWE observations have been planned for subsequent oppositions.

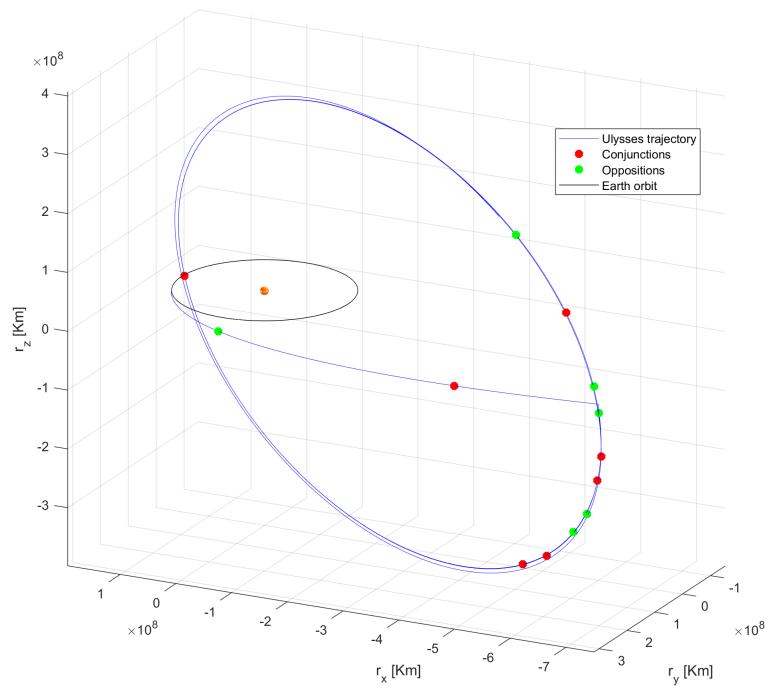


Figure 4.1: Conjunctions and oppositions

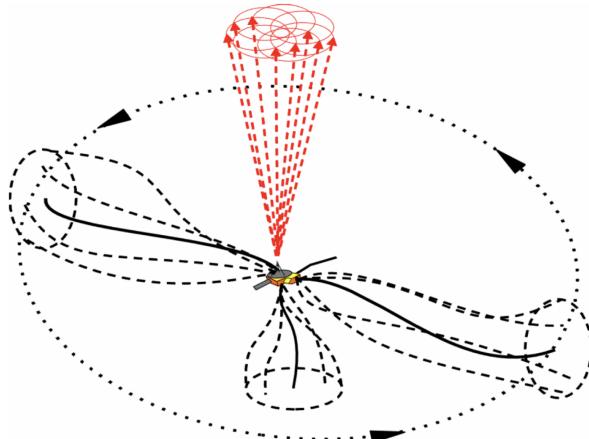
4.6.2 Possible eclipse during Jupiter's flyby

Another critical phase in Ulysses lifetime is the Jupiter flyby performed in February 1992. Using the available equations from literature [6] and ephemerides centred on Jupiter, as can be seen from figure A.11, from 5 Feb 1992 to 10 Feb 1992 we have seen that no eclipse from Earth occurred during the closest approach to Jupiter, nonetheless the TT&C subsystem experienced degraded performances due to interference from the intense magnetosphere of Jupiter and the close passage to its radiation belt.

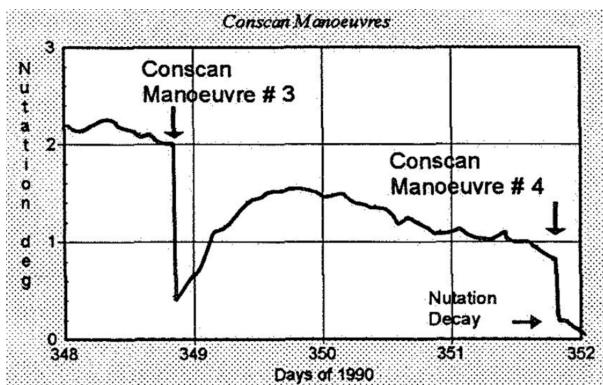
4.6.3 Nutation

The solar thermal energy causes an important dynamic disturbance, called nutation. Being Ulysses is equipped with 3 flexible booms, one 8 m axial boom aligned with the spacecraft's spin axis and two wire booms 72.5 m long in the orthogonal plane with respect to the axial boom, this disturbance causes an undesired wobbling of the spacecraft. Figure 4.2a shows the possible flexure modes of the wire booms and antennas. If no attempt were made to damp the nutation, this could cause severe damage or ultimately lead to the loss of the spacecraft since the wire booms could wrap around the main body. Furthermore, they could potentially detach, leading to massive dynamic instability. The axial boom is also potentially subject to mechanical failure.

Finally a CONSCAN manoeuvre was tried which exploits the uplink signal as a beacon to track the Earth



(a) Flexure modes of wire booms and antennas



(b) CONSCAN maneuvers during 1990

Figure 4.2: Nutation and CONSCAN maneuvers

and it was also designed to have some nutation damp properties. In fact, this manoeuvre rapidly reduced the nutation amplitude to 0.25° and to conserve this reduction it was necessary to keep it activated, having verified that fuel consumption was not excessive. The anomaly returned for year-long periods in 1994-1995, 2000 - 2001 and 2007 - 2008. During both seasons however the nutation was successfully controlled.

4.6.4 Doppler effect

Another factor that must be considered is the doppler effect induced by high relative velocity of Ulysses with respect to Earth causing a change in the signal's frequency. This effect was periodically corrected by making the opposite change in the telecommand subcarrier Frequency and Bit Rate. Furthermore, due to high distances of Ulysses from Earth, also the time delay in communication between the spacecraft and ground stations must be taken into account.

5 Attitude Determination and Control s/s

The Attitude and Orbit Control subsystem is composed by three main units:

- The Attitude and Orbital Control Electronics which uses input from the receivers, decoders, Sun sensors and ground commands to control the spacecraft spin rate, attitude and manoeuvres. It has four modes of operation: spin control, Solar Aspect angle control, Earth pointing attitude control and thrust control by telecommand.
- The Attitude Measurement Electronics process raw Sun pulses from the Sun sensors and provides most of the power switching for the AOCS. Moreover, this unit also controls the power to the valves in the Reaction Control Subsystem and to the heaters used to heat the thrusters before firing.
- The Reaction Control Subsystem which consists of all Propulsion Subsystem's parts, namely the tank, pipes, valves and thrusters that contain and regulate the flow of hydrazine. Routine attitude manoeuvres consist of pulsing an axial thruster at the correct phase in the spin cycle to slew the spin axis across the earth path.

The primary operational functions of the AOCS have the objective to maintain the spacecraft's spin axis Earth-pointing and control the spin rate. Additional operational functions are dictated by trajectory control requirements, nutation damping and by the measurement of the attitude for scientific reasons. Another AOCS operation is the periodic precession manoeuvring for correction of the apparent Earth drift with respect to the spin axis. These can be performed in closed loop on-board or in open loop via ground or time-tagged command.

5.1 Sensors

Four multiple slit Sun sensors, whose position is shown in figure 5.1, provide pulses whenever the Sun crosses their field of view during the 12 second spin cycle. These pulses are processed by the CONSCAN to provide an unambiguous Spin Reference Pulse (SRP) that provides the basis for measuring the direction of origin of many experiments, as well giving a datum from which to time thrusters firings. The Sun sensors also provide the Solar Aspect Angle (SAA), the angle between the spin axis and the satellite-Sun vector. The AOCS can perform a single closed loop control mode that can control spin rate from the SRP in case of large spin disturbances, encountered for instance during Trajectory Correction Manoeuvre where the effects of small thruster misalignments were magnified because of the long burn times necessary; and two closed loop control modes to control the SAA:

- the SAA Control mode
- Constant SAA Slew mode



Figure 5.1: Position of Sun Sensors

Both these modes were provided in order to assist in performing initial Earth acquisition in the early mission, and Earth reacquisition manoeuvres in case Earth pointing is lost later in the mission.

5.2 Accuracy requirements

Due to the fact that Ulysses spins at 5 rpm and is not in the presence of major perturbations, it is able to maintain a stable inertial attitude for long periods of time. The critical attitude control requirement is to keep the HGA foresight pointed at the Earth within about 0.5° .

The AOCS includes also failure-mode-detection and protection functions which result in fail-safe operation

and a re-acquisition capability in both automatic and ground-initiated recovery sequences. In particular, this subsystem monitors three failure protection parameters: if the SAA drifts outside the allowed dead bands, if the spin axis moves more than 0.75° from the Earth or if the spin rate drifts more than 0.2 rpm from its nominal value, a failure signal will be generated and the Reaction Control Subsystem's latching valves will close, preventing further fuel from flowing to the thrusters, and terminating the manoeuvre. Moreover, the AOCS provides autonomous system capabilities for safe spacecraft reconfiguration, which is required during unexpected and/or predicted periods of no-tracking and because of the long time needed by the signal to travel between ground and spacecraft. Other inherent functions are search-mode initiation to reacquire the Earth if no command is received after a determined time of up to 30 days, switch-over of redundant units, and programmed attitude manoeuvres at superior conjunctions.

5.3 Thrusters configuration

As previously stated in the propulsion subsystem, Ulysses is a spin stabilized spacecraft equipped with 8 catalytic thrusters mounted on +X and -X wing that provide control on the spinning angular velocity and on the direction of the spin axis. Additional details on the thrusters specifications are briefly resumed in table 3.1

The configuration of the actuators is chosen in order to guarantee complete control of the system with the minimal number of thrusters so that lightness, simplicity and reliability are favoured. Four thrusters are responsible for the control of the spinning angular velocity to ensure redundancy in case of failure.

5.4 Attitude determination

Given a set of inertial reference vectors and a corresponding set of angular measurements between a body axis and these reference vectors, the problem of single axis attitude determination can be formulated as a linear least squares problem with norm constraint on the solution (LSQN). [7] The LSQN formulation is applied to attitude determination for Ulysses from Sun aspect angle and Conical Scanning measurements. It is implemented in the Flight Dynamics system as set of subroutines, callable via an interactive program and via the Ulysses real-time monitor program.

5.5 Attitude analysis

In order to size the attitude manoeuvres required by Ulysses a simplified Simulink model has been implemented. For simplicity the inertia matrix is considered constant over time due to the fact that the time span associated to the manoeuvres is relatively small with respect to the total lifetime of the spacecraft and moreover an intrinsic margin has been considered by overestimating the spacecraft's masses and dimensions.

After the injection in the transfer orbit, Ulysses detaches from the PAM/IUS and starts its journey towards Jupiter. Due to stabilization purposes, the spacecraft rotates around its spin axis at 80 rpm (8.4 rad/s) and it is not pointing Earth making communications through High Gain Antenna impossible. In order to establish a link with the Ground Stations the spacecraft must reduce its angular velocity to the nominal value of 5 rpm and then gradually change its orientation in space to achieve Earth pointing.

Ulysses is also subjected to Solar Radiation Pressure disturbance, which generates undesired torques around the centre of mass of the spacecraft when incident sunlight is present. These torques are several orders of magnitude smaller with respect to the ones produced by hydrazine thrusters and tend to decrease over time since the spacecraft proceeds towards the outer part of the solar system, nonetheless they must be considered since, due to the long-time of action, they can affect in a non-negligible way the orbit and attitude of the spacecraft.

The sensors and actuators error induced during the simulation are modelled as an orthonormal matrix composed by a constant bias error matrix and a random error matrix simulating electro-mechanical noise and thrusters misalignment through filtered white Gaussian noise with zero mean and standard deviation

defined by the instrument's specifications.

In general, attitude manoeuvres are divided in three different modes: Detumbling, Slew manoeuvre and Tracking; that will be discussed in the following paragraphs. As previously mentioned, Ulysses relies only on hydrazine thrusters with a maximum thrust of 2 N, consequently the manoeuvres must be completed in a large time window in order to obtain feasible control torques.

5.5.1 Detumbling mode

The detumbling mode consists of a closed-loop linear control law with the aim to decrease the angular velocity of the spacecraft from an initial value to the desired one. The control law presents only a proportional gain coefficient $k_{\text{detumbling}}$ that multiplies the error between the actual angular velocity of the spacecraft and the desired one, as shown in equation 5.1.

$$\vec{M}_{\text{detumbling}} = -k_{\text{detumbling}}(\vec{\omega} - \vec{\omega}_d) \quad (5.1)$$

As previously mentioned, the desired angular velocity is 5 rpm around the High Gain Antenna boresight and shall also take into account that the Earth moves over time following its path around the Sun. The gain is set to 0.25 and the convergence is achieved in $50 \cdot 10^3$ seconds.

5.5.2 Slew maneuver mode

After the convergence of the angular velocities the slew manoeuvre begins making the orientation slowly changing over time to match the desired one. In order to point Earth, the z-axis of the spacecraft must coincide with the vector that connects Ulysses and the Earth. The control law adopted is nonlinear proportional/differential, as shown in equation 5.2, and the gains that multiply the error in the angular velocity and in the orientation are set respectively to 100 and 0.05.

$$\vec{M}_{\text{slew}} = -k_{\text{slew}_1}(\vec{\omega} - \vec{\omega}_d) - k_{\text{slew}_2}(\mathbf{A}_e^T - \mathbf{A}_e)^V \quad (5.2)$$

Considering the control law adopted, convergence is obtained in $150 \cdot 10^3$ seconds. Finally, at the end of the manoeuvre Ulysses can establish for the first time a direct link with Earth through the HGA.

5.5.3 Tracking mode

When the slew manoeuvre is switched off the tracking starts. The latter provides a fine control minimizing the pointing error and keeping the satellite spinning with a minimal fuel consumption. The control law is also in this case nonlinear proportional/differential and the gains are both set to 1.

$$\vec{M}_{\text{tracking}} = -k_{\text{tracking}_1}(\vec{\omega} - \vec{\omega}_d) - k_{\text{tracking}_2}(\mathbf{A}_e^T - \mathbf{A}_e)^V + \vec{\omega} \times \mathbf{I}\vec{\omega} \quad (5.3)$$

5.6 AOCS results

The results are obtained analysing different initial orientations of the spacecraft after the detachment from PAM/IUS. In particular, angular velocities, pointing error and deltaV are briefly discussed in the following paragraphs.

5.6.1 Angular velocity

As it is possible to see from figure 5.2, the component z of the spacecraft's angular velocity decreases during the detumbling mode and converges to the desired value which is kept constant by slew manoeuvre and tracking mode. The x and y component are always almost zero since the relative drift of the Earth with respect to Ulysses is much smaller than the angular velocity around the spin axis z. The analysis highlights that the evolution over time of the three components is affected in a negligible way by the initial orientation of the spacecraft.

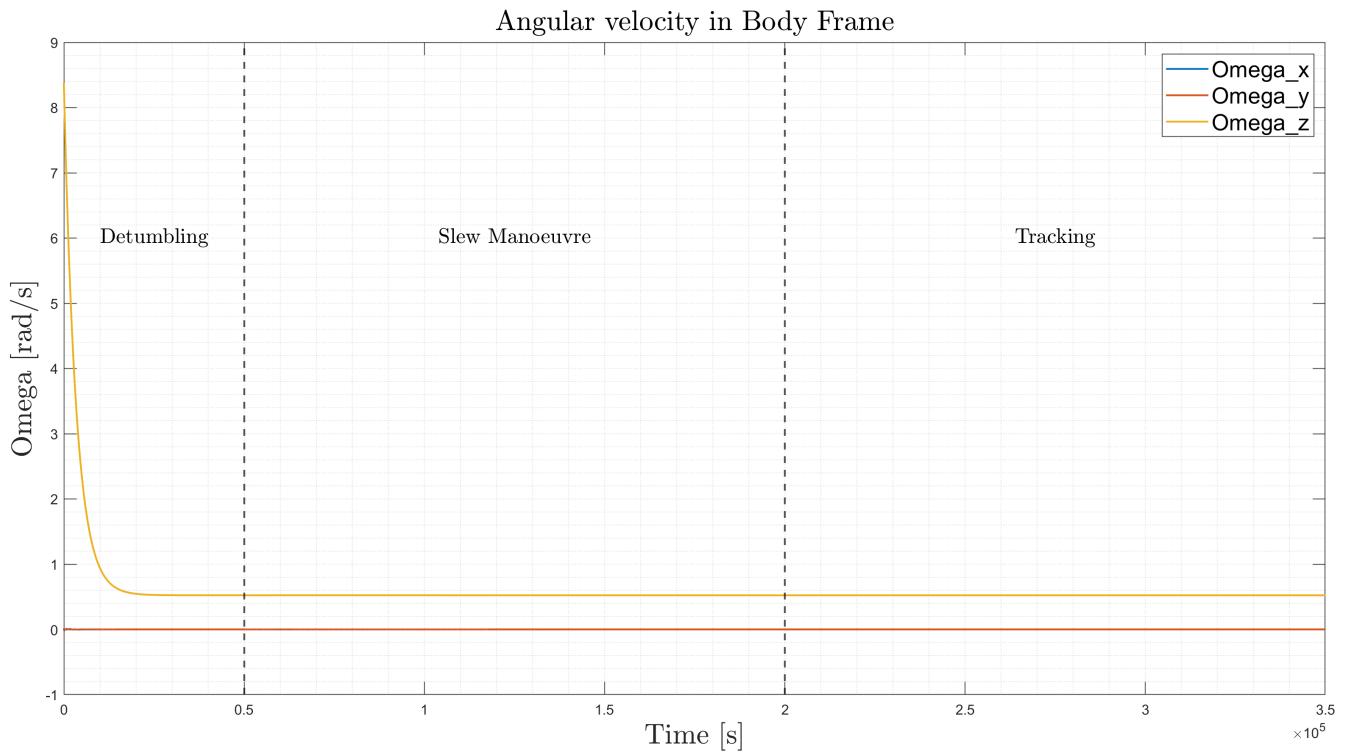


Figure 5.2: Angular velocity components variation with time

5.6.2 Pointing error

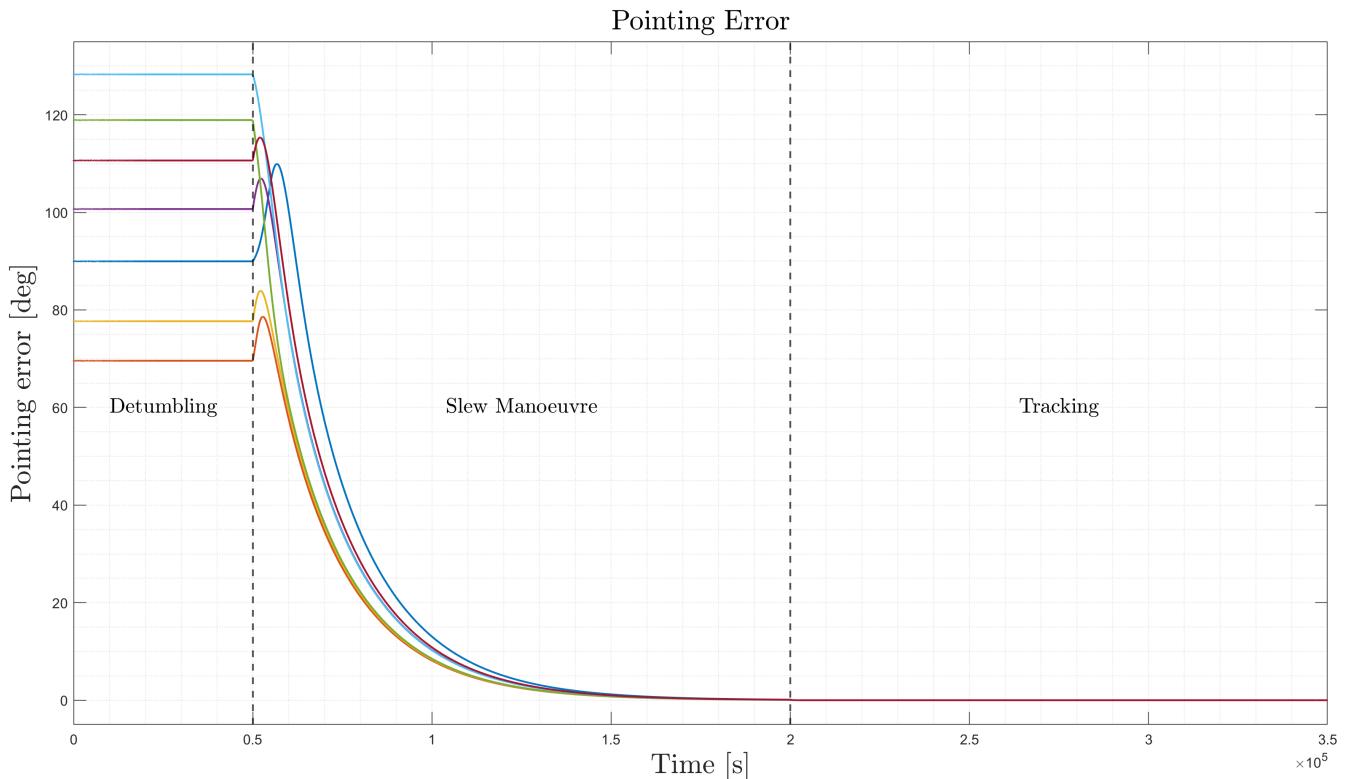


Figure 5.3: Pointing error variation with time

Since the pointing error is the angle between the spin axis z and the Ulysses-Earth vector, its initial value is influenced by the orientation of the spacecraft in space at the beginning of the detumbling mode. During this manoeuvre the pointing error remains in general constant, while as the slew manoeuvre begins it starts converging to zero, even though for some orientations the pointing error initially shows a temporary increment. Finally, the tracking mode starts ensuring that this value is always kept below 10^{-3}° , fulfilling the requirement of guarantee at least 0.5° in pointing accuracy.

5.6.3 ΔV

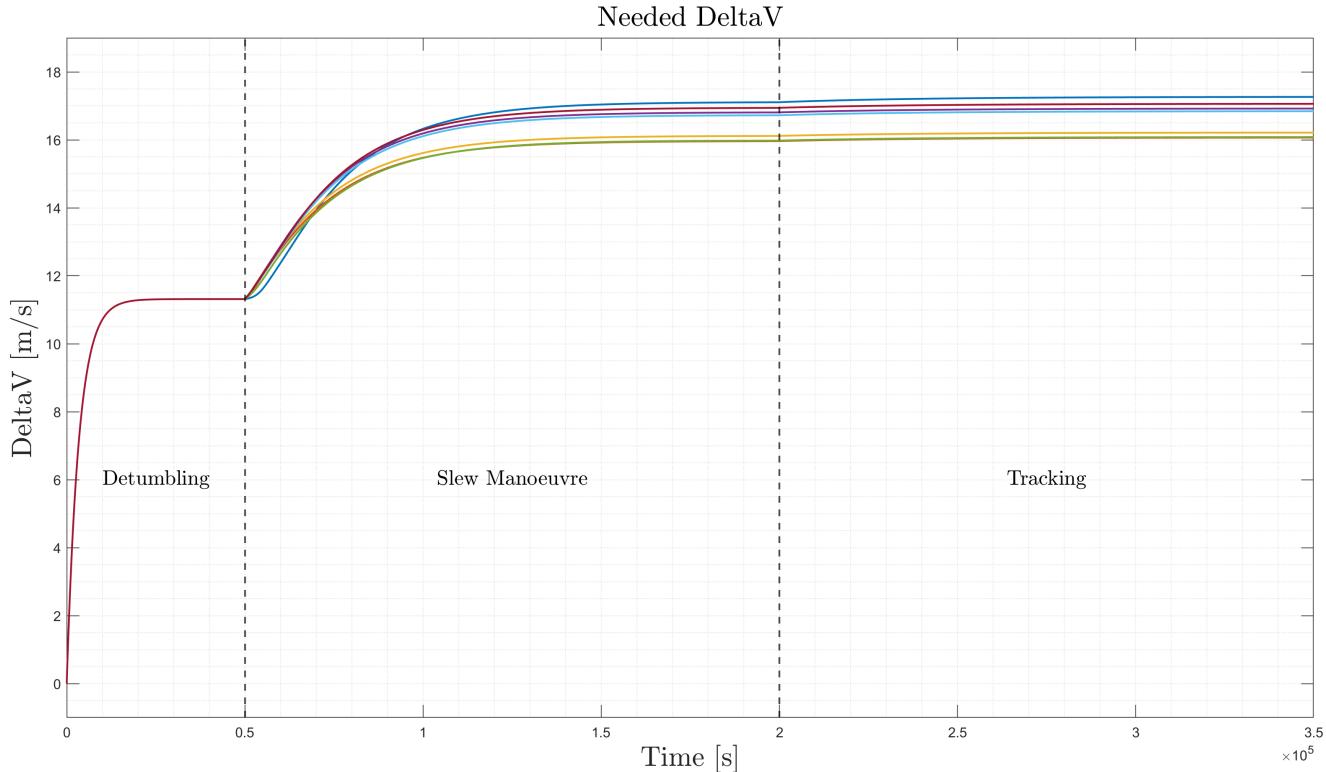


Figure 5.4: ΔV variation with time

For all the orientation analysed the ΔV required for the attitude control manoeuvres increase rapidly at the beginning of the detumbling mode and slew manoeuvre since the torques required are high, then they stabilize to a constant value as the phases converge. In the initial phase the results coincide since the ΔV derives from braking torques needed to achieve the angular speed of 5 rpm which does not depend on the orientation in space. During the tracking mode the increase in the ΔV is linear with a minimal slope since the torques required to maintain the desired attitude and angular velocity are in the order of 10^{-4} Nm. After $350 \cdot 10^3$ seconds the total ΔV for the attitude control manoeuvre ranges between 16 m/s and 17.3 m/s, which corresponds to a maximum of 2.9 kg of hydrazine needed. As shown in figure 5.4, the final values do not dramatically change with the initial attitude and are compatible with the global ΔV budget for corrections of 0.1327 km/s evaluated during the mission analysis.

To sum up, table 5.1 briefly illustrates the main results of the attitude analysis.

| Modes | Starting time | Ending time | Maximum torque | Maximum ΔV | Margins |
|-------------------|---------------|-------------|----------------|--------------------|---|
| | [s] | [s] | [mN · m] | [m/s] | |
| Detumbling | T+0 | T+50000 | 2000 | 11.31 | A 100 % margin has been considered for stochastic maneuvers and a 10 % for deterministic ones. A 50 % margin has been considered in the inertia matrix. |
| Slew | T+50000 | T+200000 | 100 | 5.79 | |
| Tracking | T+200000 | - | 4 | - | |

Table 5.1: Main results of the attitude analysis

5.7 Possible alternatives

5.7.1 Reaction wheels and CMGs

A possible alternative to hydrazine thrusters for attitude control are reaction wheels. These actuators are based on acceleration and deceleration of a spinning rotor thanks to an electric engine and provide a precise control, especially for pointing.

The major problem is that reaction wheels can't produce net torque but only exchange angular momentum with the spacecraft. Furthermore, like any electric motor, they can reach the saturation speed making the torque exchanged fall to zero. This means that reaction wheels shall be accompanied by another set of actuators that must operate in order to desaturate them and, at the same time, continuously control the spacecraft. So, even if reaction wheels and, in the same way, inertia wheel and control moment gyros, represent a possible choice for actuators they imply a great increasing in the complexity of the system and consequent reduction of the reliability.

5.7.2 Ion thrusters

Ion thrusters provide high specific impulse and low continuous thrust through the ejection of ionized gas ensuring a minimal fuel consumption. Unfortunately, in the 90s this technology was not fully developed and was never adopted for interplanetary mission.

6 Electrical power s/s

6.1 Subsystem description

The electrical power subsystem has the duty to provide electrical power to feed the on-board instrumentation, for their correct functioning, and the thermal power (through dampers and heaters) to maintain adequate temperatures in each part of the spacecraft. The architecture is made by several components allocated over a bus, through which the current flows and power can be distributed. Additional details will be discussed in the following paragraphs.

6.1.1 RTG

More specifically, Ulysses used a Radioisotope-Thermoelectric-Generator (RTG) to provide the power demanded in order to complete the mission. In general, RTGs provide power through the natural radioactive

decay of a radioisotope, ^{238}Pu in the form of plutonium (IV) oxide (PuO_2) for Ulysses. The thermal energy generated by this natural process is then converted to electric energy by solid-state thermo-electric converters. Furthermore, the choice of an RTG is driven by the fact that it allows the spacecraft to operate at a significant distance from the Sun, regions where solar panels cannot provide the required power.

In the particular case of Ulysses' RTG, the 4500 W of thermal energy are converted by a Si-Ge converter into 289 W of electric power at the beginning of the mission. It's important to note that the electric power is not constant during the mission's lifetime and it was planned to be 250 W at nominal mission end.[8] The choice of the radioisotope in an RTG for space applications is driven by three main factors:

- The radio-isotope half life must be long enough in order to guarantee a relatively constant power output for a reasonable amount of time. (i.e. the thermal power shall not decay drastically in the mission's lifetime)
- The power density must be high enough in order to grant both the needs of saving mass on board and of the electrical power output.
- The radiation emitted by the decaying process must be easy to shield. Consequently, radio-isotopes emitting the least gamma, neutron and, in general, penetrating radiations are preferred.

Table A.6 briefly lists all these previously described characteristics for some of the most used radio-isotopes for RTGs.

The choice of ^{238}Pu is driven by its reasonable power density of 0.41 W/g and is one of the best radioisotope in terms of low radiation shielding requirements, meeting the criterion to need less than 25 mm of lead shield in order to block the radiation. In particular, ^{238}Pu needs only 2.5 mm of lead shielding making usually its case adequate to avoid radiation contamination. ^{210}Po , as well as ^{242}Cu , would be good candidates in terms of power density and radiation shielding but it's really low half-life time makes it unfeasible for a long time mission as Ulysses. The other possible candidates analyzed in table A.6 either have an half-life that is too low for a long term mission or the shielding requirements become critical.

6.1.2 IPDs and EPDs

Most of Ulysses' power is used to run subsystems and science instruments. Any power that is not immediately needed is routed to 12 Internal Power Dumpers (IPDs) which are resistances distributed inside the spacecraft thermal enclosure. Their role is to regulate power and providing general heating to the fuel lines, fuel tank and electrical units, which need a stable thermal environment. Power dumped in IPDs is controlled to maintain the spacecraft Main Bus Voltage within a 2% tolerance of 28V under all operational conditions.

On the other hand, considering the relatively high eccentricity of Ulysses' trajectory around the Sun, the solar heating input on the spacecraft can be between 45 W/m² at aphelion to about 1300 W/m² at perihelion. During the hottest phases of the mission, the power dumped to the IPDs can excessively increase temperatures inside the spacecraft thermal enclosure. External Power Dumpers (EPDs) are in this way mounted outside the spacecraft to radiate excessive electrical power not needed for heating. The choice of how much power to dump externally is made on the ground by the Flight Control Team at JPL. EPDs can be switched by telecommand in combinations of 10, 20, 40, 50, and 100W.

6.1.3 Platform heaters

The spacecraft uses heaters in order to provide local heating to units that are exposed to low temperatures during phases of the mission when the spacecraft is far from the Sun. Special attention is given to any fuel-bearing component, as hydrazine freezes at approximately 2 °C and can become unstable when thawed. Units that are outside of the spacecraft's thermal enclosure are also of concern (e.g. Sun Sensors). The following paragraphs explain in detail the different types of heaters on-board of Ulysses.

6.1.3.1 Hot case heater Heats the coldest sections of the Reaction Control Subsystem. This heater was switched on after Ulysses deployment from the Shuttle and has only been switched off for a brief period during the early mission since then. The heater dissipates a total of 8.9 W to:

- Fuel tank, hydrazine fill and vent valve
- the X wing pipelines and the two thrusters blocks

The denomination 'Hot Case' comes from its use. More specifically, it was designed to be employed during the mission's hottest phases

The Hot Case Heater current is monitored by a Saturation Detector, as shown in figure ???. If this circuit drops below rated power for more than 24 seconds, the Saturation Detector disconnects the payload from the Main Bus by opening the Main Switch. Since the payload science instruments consume about 55W, this action, performing a Disconnect Non-Essential Loads (DNEL), should restore sufficient power to ensure heater saturation.

6.1.3.2 Cold case heater The Cold Case Heater heats the sections of the RCS and spacecraft exposed to low temperatures, when the spacecraft is sufficiently far from the Sun not to keep the components warm by solar heating. This heater is generally switched on when the spacecraft is beyond about 2AU from the Sun. However the decision is made based on component temperatures on the spacecraft, not on distance. The heater dissipates a total of 24.9W to:

- the central pipelines inside the spacecraft thermal enclosure
- the latching valves
- pressure transducers and filters
- the X-wing pipelines
- the two thruster blocks.

On the same rational of the previous one, it is called the 'Cold Case' heater because it was designed for use during the mission's coldest thermal case.

6.1.3.3 X-wing heater The Wing Heaters are located on the thruster blocks and are exclusively for heating that local area. Two of them are present on board, the +X and -X Wing heater and dissipate respectively 1.4W and 1.8W respectively, and are each capable of raising the thruster block temperatures of about 10°C. These heaters can be switched independently, as for scientific reasons it is important to keep the wing temperatures within 10°C of each other. However, in practice it is found that the thruster block temperatures usually are in the range 2°C and the heaters can be switched together when it is necessary to warm or cool the blocks.

6.1.3.4 Longeron heater The Longeron Heater is installed on the -X/+Y longeron, near the hydrazine fill and vent valve bracket. This heater was meant to compensate for heat loss to the Shuttle Payload Adapter during the launch phase, avoiding freezing of the valve. This heater was specifically designed for the launch phase and subsequently was no longer used afterwards.

6.2 RTG power decay

As previously mentioned, the RTG converts 4500W of thermal power obtained by the radioactive decay of ^{238}Pu into electric power. The electrical power output is not constant through the RTG's lifetime as a result of two factors:

- Fuel decay
- Thermoelectric degradation

In order to perform all of the task the RTG needed to fulfill requirements on the power at begin of mission (BOM) and at nominal mission end, shown in table 6.1.

| Electrical power | Value |
|--------------------------|-------|
| P_{BOM} | 289 W |
| $P_{\text{nominal-EOM}}$ | 250 W |

Table 6.1: RTG electric power requirements

6.2.1 RTG performances estimation

A general method to predict the variability of the output of an RTG electrical power output is described in the following. A firstly simplified model can be derived by considering only the effect on fuel decay. The RTG's thermal power at any time of the mission t can be calculated with the following exponential:

$$Q(t) = Q_0 e^{-\lambda t} \quad (6.1)$$

where: Q_0 = thermal power at the begin of mission

λ = ^{238}Pu decay constant which is then related to its half time τ as in $\lambda = \ln(2)/\tau$

Considering these simplifications, it is possible to obtain an expression of the effect of fuel degradation on the RTG's power output (i.e. electrical power):

$$\frac{P(t)}{P_0} = 1 - \frac{1 - e^{-\lambda t}}{1 + \frac{P^*}{\eta^* Q_0}} \quad (6.2)$$

where: P_0 = electrical power at BOM

η^*, P^* = coefficients that depend on the RTG's thermal environment

On the other hand, by using this simplified approach the electrical power output at nominal EOM is approximately 269 W, which is not compliant with the real values illustrated in table 6.1. Subsequently, a more refined model needs to be used.

A model that takes into account the effect of thermo-electric degradation (in addition to the fuel decay) can be built. Predicting the thermo-electric degradation with time is in general a complex problem since it involves many degradation mechanisms. A very detailed method is the DEGRA code developed by V.Raag [9] which has an analytical solution shown below in equation 6.3.

$$P = (P^* + \eta^* Q_0 e^{-\lambda t}) \left\{ 1 - \sqrt{\frac{e^{-\frac{T^*}{T_1}} - e^{-\frac{T^*}{T}}}{\lambda t^* \frac{T^*}{T_0} \left(1 - \frac{T_0}{T_1}\right)}} \right\} \quad (6.3)$$

where: T^*, t^* = empirical values describing thermo-electric degradation

T_1 = $T_0 + \alpha Q_0$

T = $T_0 + \alpha Q_0 e^{-\lambda t}$

α, T_0 = coefficient depending on the RTG's thermal environment

With this model in mind, the electrical power output at nominal EOM is estimated to be approximately

247 W, which is coherent with the value shown in table 6.1. This is also confirmed by the satisfaction of the August 1995 nominal EOM power requirement to be higher than 245 W from which the mission was successfully extended.

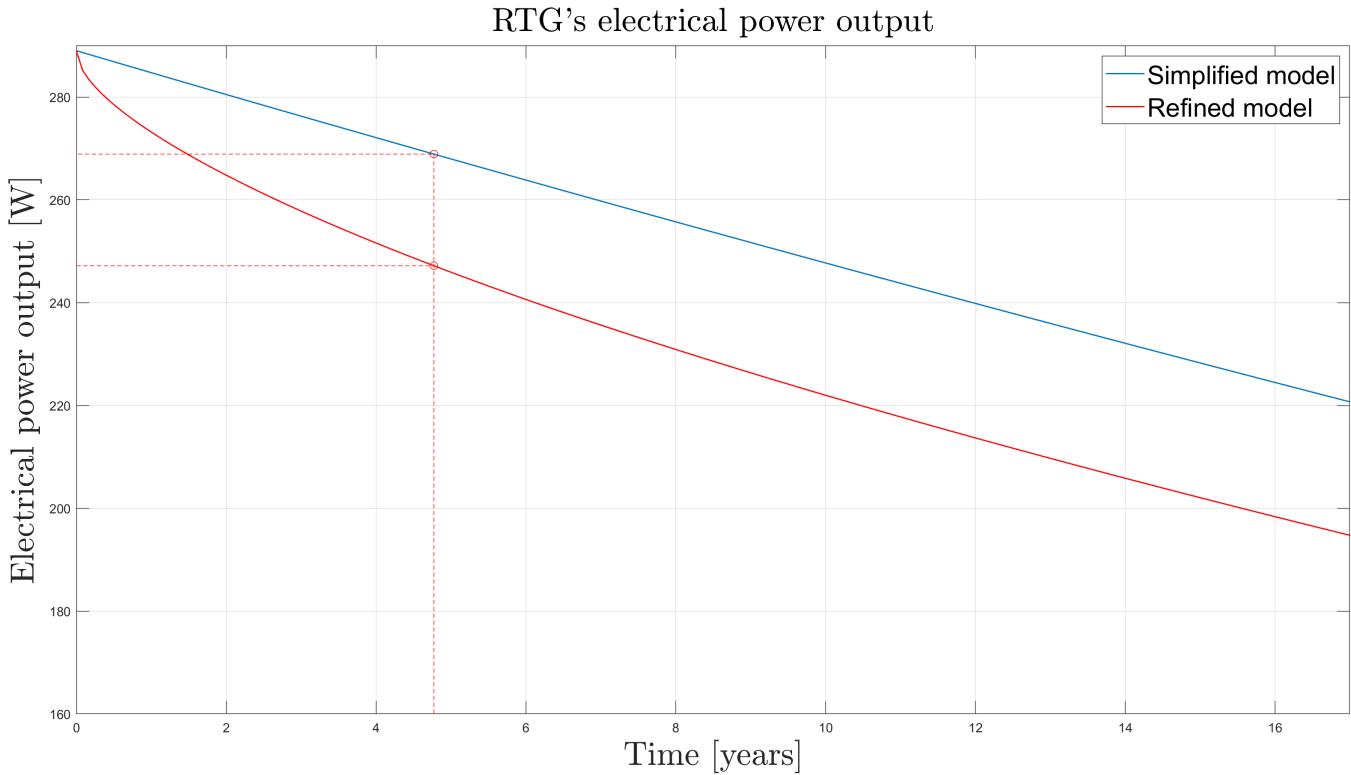


Figure 6.1: Estimated RTG power output with time

6.2.2 Mass of ^{238}Pu estimation

In order to estimate the mass of plutonium needed to successfully achieve the requirements to having a nominal mission life of 5 years, equation 6.3 can be used to derive the thermal power at begin of mission Q_0 , which is the only unknown parameter.

More specifically, considering the power density of PuO_2 being 0.41 W/g, Q_0 can be easily derive from which the mass of plutonium can be automatically calculated. Table 6.2 illustrates the results of these calculations compared to the real data of the mission.

| Quantity | Estimated value | Real value |
|-----------------|-----------------|------------|
| Q_0 | 4543 W | 4500 W |
| m_{Pu} | 11.08 kg | 11 kg |

Table 6.2: Mass of plutonium estimation results

As it is possible to see, the table hereabove shows that the estimated quantities are coherent with the real ones.

6.3 EPS power budget

For every phase of the mission the power budget has been estimated and compared to the RTG's power output at nominal EOM, as shown in table 6.3. A 20 % margin has been considered in the analysis in

| Phase | Margin | P_{required} [W] | RTG power output _{NEOM} [W] |
|-------------------------|--------|---------------------------|--|
| Interplanetary transfer | | 205 | |
| Flyby | 20 % | 185 | 250 |
| OOE | | 222 (pericenter) | |
| | | 248 (apocenter) | |

Table 6.3: Power budget for each phase compared to the RTG's power output

order to take into account the uncertainty if some instruments were actually active during the specific phase. The specific value is a result of a comparison between the peak and mean power output of every instrument and the actual available electric power from the RTG.

The analysis highlights that the power required is lower than the one generated by the RTG at nominal EOM for each phase. More specifically, the highest power required by the spacecraft is during the OOE phase. This is mainly due to the fact that this is the phase where all the instruments are active, in contrast with the other ones where very few instruments are switched on. It's also important to note that the power demanded at the apocenter is higher than the one at the pericenter mainly due to the Cold-Case Heater having an high power demand.

7 Thermal control s/s

Thermal control of the spacecraft, its subsystems and of most of the experiments is achieved by passive means in conjunction with a commandable internal/external power dump and heater system. This involves an optimised layout of subsystems which avoids hot spots on the spacecraft platform, an efficient thermal-blanket design in order to minimise the solar input, the compensation, by the power dump system, of heat fluxes which are caused by the varying solar input and a heater system for individual critical units.

7.1 Multi-layer insulation

Multilayer Insulation (MLI) blankets provide a lightweight insulation system with a high thermal resistance in vacuum. MLI blankets are utilized to reduce heat loss from a spacecraft to the cold space, or to prevent excessive heating of the surroundings from an internal component with heat dissipation.

The radiation shields are generally a plastic film metalized on either one side or both sides of the film. The principle of an MLI blanket is to use multiple layers of radiation shields to reflect back, in the opposite direction of heat flow, a large percentage of the radiant heat flux reaching each radiation shield. MLI is therefore very effective if solid conduction through the spacers and gaseous conduction through the gas medium can be minimized.

MLI blankets typically consist of three to thirty layers of metalized plastic sheets. The inner layers are typically as thin as possible to minimize weight and are usually made of aluminized Mylar or Kapton, separated by spacers. The innermost and outermost layers of the blanket, however, are usually made of thicker aluminized Kapton which provides protection during installation and handling. Thermal control laminates can also be used as the outermost layer for additional toughness.

7.2 Temperature estimation

The most stringent requirements on the thermal subsystem are to always guarantee a temperature above +5 °C for the hydrazine of the Attitude and Orbit Control Subsystem (AOCS) and a temperature below +35 °C for all experiment solid-state detectors. All spacecraft walls are covered with thermal multi-layer blankets, which are closely fitted around the experiment-sensor apertures. The blankets consist typically of 20 layers of aluminized mylar. The outermost layer is kapton, coated with a transparent conductive coating (Indium Tin Oxide) to provide an electrically conductive outer spacecraft surface. Heat rejection is performed by a thermal radiator, located on the rear of the spacecraft and covered by a 2 mil kapton foil. All units external to the spacecraft (e.g., several experiments) are thermally decoupled from the interior. Following this reasoning, the temperature range identified for the the spacecraft with the relative margin is reported in the follwing table.

| Quantity | Value | Margin | Value after margin |
|-----------|---------|-------------|--------------------|
| T_{min} | + 5 °C | ± 10 °C | 15 °C |
| T_{max} | + 35 °C | | 25 °C |

Table 7.1: Temperature requirements and relative margins

In order to characterize the temperature of the spacecraft we need firstly to define the power inputs that are acting on the spacecraft in the two main phases: interplanetary transfer and OOE.

7.2.1 Transfer orbit

In this phase, given the geometry of the trajectory, the hot case is defined as the moment of departure from the parking orbit, while the cold case is during at the spacecraft's maximum distance from the Sun (i.e. before Jupiter's flyby).

7.2.1.1 Hot-case scenario In these case, since we are in a parking orbit close to Earth, planetary albedo and IR radiation, that follow an inverse square law with the distance from the planet, are non-negligible. Furthermore, also the Sun's radiation is present and strong due to the close vicinity to it. For this reason the power balance on the spacecraft is:

$$A_e \sigma \epsilon (T_{sc}^4 - T_{space}^4) = A_\odot \alpha \Phi|_{1AU} + a_\oplus A_\oplus \alpha \Phi|_{1AU} \left(\frac{R_\oplus}{R_\oplus + h_{po}} \right)^2 + A_{IR} \sigma \epsilon_\oplus T_\oplus^4 \left(\frac{R_\oplus}{R_\oplus + h_{po}} \right)^2 \quad (7.1)$$

where: ϵ = Emissivity

A_\odot = Area of absorption of solar flux

α = Absorbivity

Φ = Solar flux

a_\oplus = Albedo factor of Earth

A_\oplus = Area of absorption of Earth's albedo

h_{po} = Height of the parking orbit

A_{IR} = Area of absorption of Earth's infrared emission

7.2.1.2 Cold-case scenario On the other hand, the cold case scenario being at approximately 5 AU, the Earth is too far away to have an influence in terms of albedo and IR radiation, for this reason we neglect these inputs. The Sun's radiation is still present even though it's approximately 1/25 of the one in

the Hot case scenario. For these reasons, we are expecting a significantly lower temperature with respect to the cold-case. For the considerations previously stated, the power balance in this scenario is:

$$A_e \epsilon \sigma (T_{sc}^4 - T_{space}^4) = A_{\odot} \alpha \Phi |_{5AU} \quad (7.2)$$

Moreover, it's also important to note that the flyby wasn't chosen as the cold-case scenario due to the fact that in this phase Jupiter's albedo and planetary emission would give additional inputs to the spacecraft that would increase its temperature.

7.2.2 OOE

In this phase, the inputs of planetary emission and albedo are not present due to the lack of any close approach to any of the Solar's system planets. For this reason, the hot and cold cases are simply identified respectively by the closest and farthest points from the Sun of the orbit (i.e. aphelion and perihelion). The computation for the equilibrium temperature is shown in the following two equations.

$$A_e \epsilon \sigma (T_{sc}^4 - T_{space}^4) = A_{\odot} \alpha \Phi |_{1.34AU} \quad \text{Hot-case scenario} \quad (7.3)$$

$$A_e \epsilon \sigma (T_{sc}^4 - T_{space}^4) = A_{\odot} \alpha \Phi |_{5.40AU} \quad \text{Cold-case scenario} \quad (7.4)$$

7.3 Results

Given the assumptions made in the previous sections, all the equilibrium temperature for each phase can be identified and are reported in table 7.2.

| Phase | Case | Temperature |
|----------------|------|-------------|
| Transfer orbit | Hot | + 158 °C |
| | Cold | - 105 °C |
| OOE | Hot | + 55 °C |
| | Cold | - 111°C |

Table 7.2: Equilibrium temperatures for each phase

The table hereabove justifies the need for heaters and radiators in order to maintain the spacecraft's temperature in the ranges defined in table 7.1. In order to do so, we take the worst situation both for cold and hot cases.

In terms of the cold case, the heaters power can be easily calculated by imposing as the spacecraft's temperature as the minimum acceptable of +15°, displayed in table 7.1.

$$A_e \epsilon \sigma (T_{min}^4 - T_{space}^4) = \sum_i Q_i + Q_{heaters} \quad (7.5)$$

where: $\sum_i Q_i$ = power inputs defined in equation 7.4.
 $Q_{heaters}$ = power generated by the heaters

Subsequently, the area of the radiators needed in the hot case can be computed by imposing the temperature of the spactraft as the maximum acceptable of +25°, displayed in table 7.1, and the one of the radiatior is the one computed in 7.2.

$$(A_e - A_{rad}) \epsilon \sigma (T_{max}^4 - T_{space}^4) + A_{rad} \epsilon_{rad} \sigma (T_{sc}^4 - T_{space}^4) = \sum_i Q_i \quad (7.6)$$

where: A_{rad} = Area of the radiator
 ϵ_{rad} = emissivity of the radiator's surface
 $\sum_i Q_i$ = Power inputs defined in equation 7.1.

Now that the area of the radiator is computed, it is needed to go back to the cold case in order to check the power needed from the heaters

$$\sigma(\epsilon(A_e - A_{rad}) + \epsilon_{rad}A_{rad})(T_{min}^4 - T_{space}^4) = \sum_i Q_i + Q_{heaters} \quad (7.7)$$

From the considerations hereabove the values for the area of the radiators A_{rad} and the power needed for the heaters $Q_{heaters}$ are computed and reported in table 7.3.

| Quantity | Estimated value |
|---------------|--------------------|
| A_{rad} | 1.1 m ² |
| $Q_{heaters}$ | 745 W |

Table 7.3: Radiatior and heaters sizing

These results are approximate since a mono-nodal analysis has been carried out. Considering that each instrument has its own temperature range which are very different from one another. For this reason, in order to get a more precise values, a multi-node analysis has to be done.

8 On board data handling s/s

8.1 Subsystem description

The Data Handling Subsystem or DHS has crucial importance because it provides all telemetry acquisition and processing, and forwards telemetry to the TTMTTC for transmission to Earth ground stations. The DHS also acquires, decodes and accepts incoming commands from the TTMTTC subsystem and distributes these commands to the instruments and platforms.

In particular, the telecommand decoder checks commands for validity and distributes them to the experiments and subsystems. When necessary, forty commands can also be stored in the space-craft time-tag buffer for later timed execution, while most of the commands are uploaded in real time.

The main component is the Central Terminal Unit (CTU) that processes command messages received from the decoder, provides onboard timing information and performs formatting and encoding of data to be sent on ground. It also controls all onboard automatic functions, including an auto-check of its own functioning. The CTU contains a master crystal oscillator from which all synchronisation and time signals for subsystems and payload are derived. 32-bit timing information with resolution

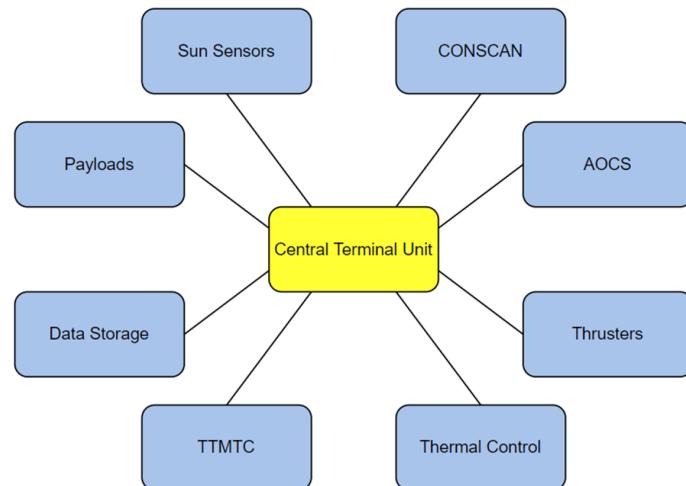


Figure 8.1: OBDH architecture scheme

of 2 seconds is included in every telemetry format, ensuring unambiguous identification of telemetry data, but the system can relay also on the Spin Reference Pulse derived through the Sun Sensors. A redundant Central Terminal Unit 2 (CTU2) is installed on the spacecraft in order to take over in case the main CTU fails, being able to process telemetry with minimum degradation.

There are three data formats: scientific format consisting of 32 scientific frames, interleaved format consisting of a block of 32 frames (selectable ratio between 1:1, 1:3 and 1:7) and finally engineering format consisting of two frames of spacecraft housekeeping data without scientific data. Telemetry channels are sampled in a time-ordered fashion and allocated to specific words (8 bit), which are arranged into frames of 128 words. Analogue channels are sampled and converted into 8 bit words with an accuracy of 1% full scale. There are also datation channels with resolution of 0.488 ms or 3.9 ms, but they are used only by the gamma ray-burst instrument (high resolution) and by the magnetometer and wave experiments (low resolution).

The described subsystem incorporates a microprocessor system with a special purpose software package specifically designed for Ulysses. Software applications monitor satellite health and safety, initiate recovery and reconfiguration, and carry out onboard data processing. Indeed, the DHS provides, in combination with the AOCS, a safe automatic manoeuvring. A variety of timing signals are also distributed for use by the other subsystems and the science instruments.

8.2 Memory storage sizing

As previously mentioned, Ulysses is tracked most of the time 8 hours per day from the DSN Ground Stations, for the remaining time it must store all the acquired data in tape recorders. The telemetry rate for the recording is set to 512 bps but can be lowered to 256 bps doubling the recording time.

| Telemetry Rate | Recording time per day | Margin | Total Memory | Real Total Memory |
|----------------|------------------------|--------|--------------|-------------------|
| 512 bit/s | 16 hours | + 300% | 84.5 Mb | 91.6 Mb |

Table 8.1: Telemetry data and memory storage sizing

A safety margin of 300 % is considered in order to avoid loss of data during prolonged periods of absence of signal that may occur especially during solar conjunctions or in case of failures in the communication system. Data are stored on two tape recorders of 45.8 Mb each.

8.3 Environmental criticality

The principal problem related to this subsystem is the environment, since the spacecraft encounters intense radiation during its mission. For instance, Ulysses shall survive at Jupiter's magnetosphere and radiation belt during planetary flyby. Furthermore, along the Out of Ecliptic Orbit the spacecraft is continuously subjected to strong solar wind.

High energy charged particles or high energy photons in a space radiation environment can cause temporary damage or permanent failure of materials and devices. Radiation damage to spacecraft mainly includes ionization or displacement damages. The first one refers to the ionization of the target atoms and the excitation of extra nuclear electrons in the material caused by incident particles, resulting in severe degradation of semiconductor devices performances. On the other hand, the latest refers to the interaction of incident particles with atoms in the material and the exchange of kinetic energy, causing the target atoms in the material to leave the original position to form interstitial atoms and create vacancies. A displaced atom may collide with other atoms multiple times, creating a shift chain.

The simplest and most effective solution is performed adopting radiation hardened materials, as shielding

for the OBDH instruments. Thus, when the charged particles interact with the nucleus or electrons of the target substances, their kinetic energy is lowered until they finally stop inside the shield and therefore don't interfere with payloads.

The major drawback of this technology is the increment of the total mass and the need to find the optimal thickness that allow high protection and simultaneously minimize second radiation production. This mentioned phenomenon refers to radiation originated from the absorption of previous radiation in matter, in the form either of electromagnetic waves or moving particles.

9 Configuration and Structure s/s

9.1 Configuration description

9.1.1 Spacecraft configuration

For the present discussion, a CAD assembly of the S/C was built in order to show precisely its configuration and later to perform the structural simulation.

The S/C consists of a box-like main body structure on which is mounted a 1.65m large-diameter high gain antenna that provides the communication link. The AOCS is responsible to keep the HGA continuously pointing earth.

From a configuration point of view , it was observed that the RTG was placed in the back of the S/C to be at the farthest position from the instruments as shown in figure 9.1 . Such position will reduce the radiation effects on the instruments and their sensors. A 5.6 m long radial boom is mounted on the side opposite to the RTG and carries several experimental sensors such as URAP, GRB, FGM, and VHM. Moreover, a 72.5 m tip-to-tip dipole wire boom and a 7.5 m axial boom that serve as electrical antennas for the (URAP) experiment are deployed from the main body of the SC to the deep space . Moreover , on the external body of the SC, 4 sun sensors are located on its upper part pointing in the same direction of the HGA.

Heat rejection is performed by a thermal radiator , located on the rear of the spacecraft, and covered by a 2 mil Kapton foil. All units external to the spacecraft (e.g. several experiments) are thermally decoupled from the interior. Additionally , there are 2 other radiators placed on the +X and -X sides of the SC which are almost always pointing toward the deeps space.

Moving toward the internal part of the S/C, most of the scientific instruments are placed on the main body far from the RTG as mentioned earlier. Additionally, the propellant tank was mounted on the main body just below the large reflector to prevent large excursions of the baricenter and moments of inertia.

In section A.17 the bill of materials explains the different callouts of the previous images.

A key scientific requirement was to have an electromagnetically and electrostatically clean spacecraft; EMC considerations have therefore driven the mechanical configuration design. The spacecraft is divided into a "quiet" and "noisy" zone.

The "quiet" comprises an electromagnetically shielded compartment of sensitive experiments, whereas the "Noisy" contains the less susceptible - but more emissive - electrical spacecraft subsystems.

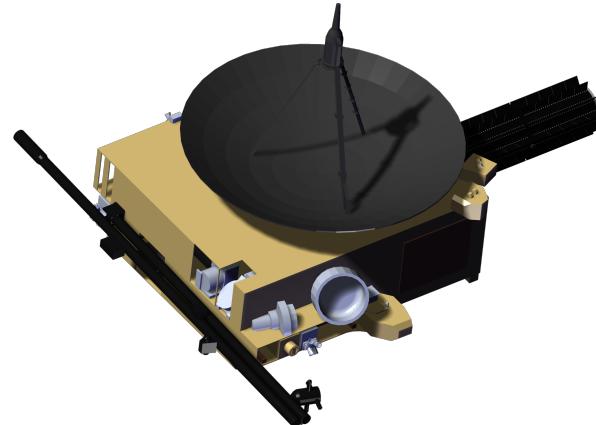


Figure 9.1: CAD Assembly of the S/C in launch configuration

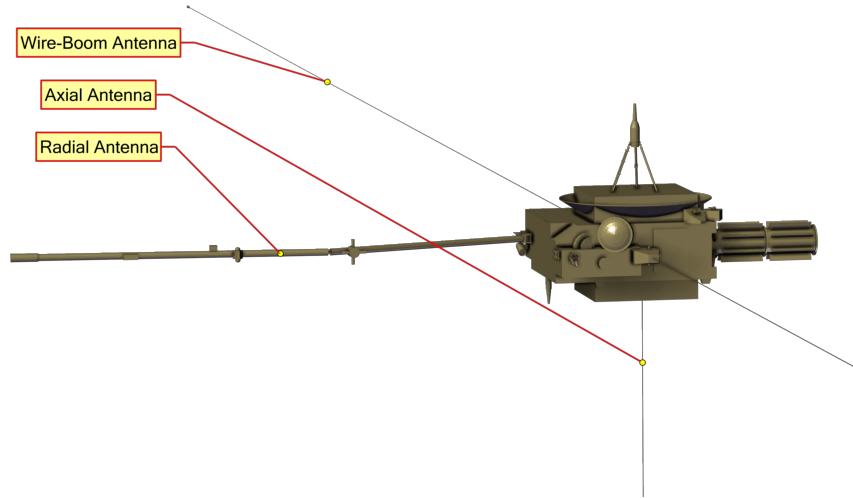


Figure 9.2: Representation of the S/C in flight configuration, from NASA 3D Resources

9.1.2 Launch configuration

In order to launch the S/C to space, several components need to be retractable or deployable in order to fit inside the space shuttle envelope as shown figure 9.3.

The 5.6 m boom is foldable but remains on the external part of the SC. Such design will put the boom under both vibrations and inertial stresses. Moreover, the other three antennas are retracted inside the S/C during launch, so they are not exposed to any direct stresses.

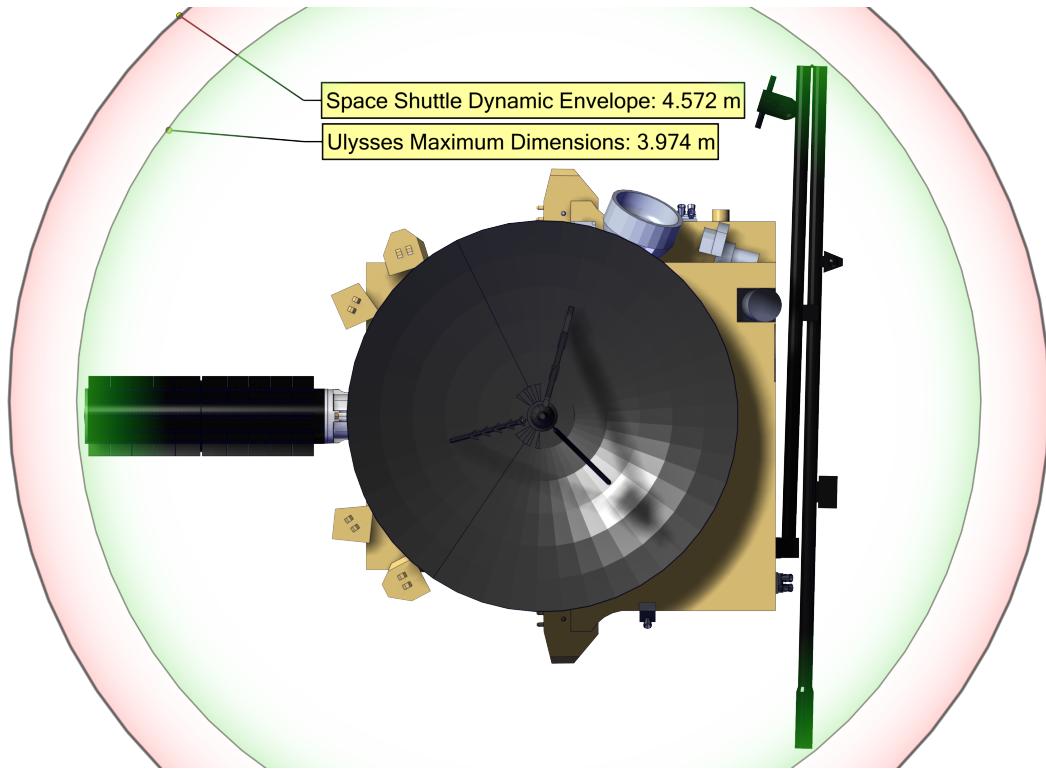


Figure 9.3: Comparison between the dynamic envelope and the maximum dimensions

The 4 squared pillars on the bottom of the S/C are connected directly to the PAM structure in the upper stage. This prevents the direct stresses on the bottom part of the SC where the radiator is located.

Additionally, the RTG is fixed and held by a metallic structure connected to the PAM in order to support its tip so avoiding excessive bending and shear stresses.

9.2 Spacecraft structure

The Ulysses spacecraft has a box-type structure with two wings on the sides and a single aluminum honeycomb equipment platform. All spacecraft walls are covered with thermal multi-layer blankets, which are closely fitted around the experiment-sensor apertures. The blankets consist typically of 20 layers of aluminized mylar. The outermost layer is Kapton, coated with a transparent conductive coating (Indium Tin Oxide) to provide an electrically conductive outer spacecraft surface.

The boom is made from carbon-fiber-reinforced plastic (CFRP) tubing 50 mm in diameter and with 1 mm wall thickness. Its design provides the maximum boom-length consistent with a two-hinge system and satisfies the spacecraft balance constraints in both the stowed and deployed configurations. On the other hand , the wire booms consist of 5 mm wide, and 0.04 mm thick Cu-Be ribbon stowed during launch on two identical drive units. The wires were deployed to a length of 72.5 m tip-to-tip by centrifugal forces acting on tip masses after the second trajectory correction maneuver (TCM-2).

The 4 previously mentioned pillars run through the whole square box of the SC , and they withstand the launch stresses for the whole structure when connected to PAM-IUS.

The whole SC body is supported by an internal truss configuration in order to ensure suitable stress distribution during nominal operations.

9.3 Structural analysis

Considering the nominal lifetime of the mission, the maximum stresses are observed during the launch in the ascent phase of the Space Shuttle. According to NSTS 21492 [10] Space Shuttle Program Payload Bay Payload User's Guide and Shuttle Orbiter/Cargo Standard Interfaces ICD-2-19001 [11], the maximum load factors during launch were equivalent to 3 g on each direction. So, a structural analysis based on the Von Mises stress criterion was done considering a total load factor of $3\sqrt{3}$ g which is equal to 18500 N.

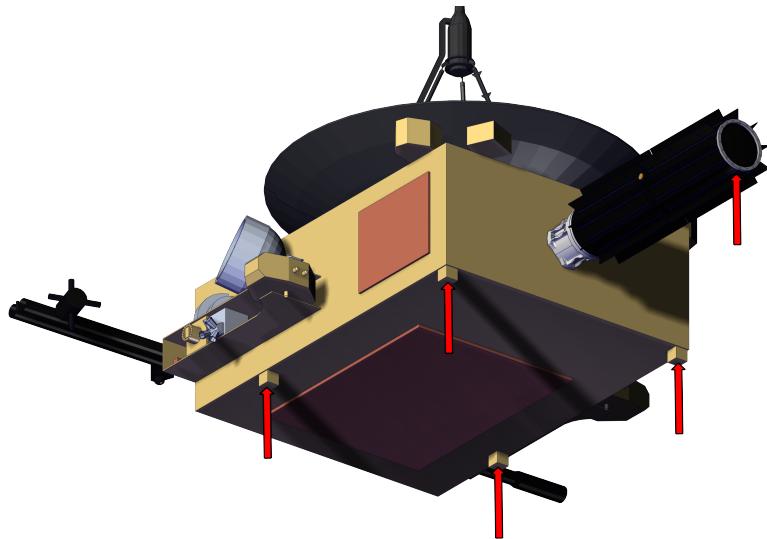


Figure 9.4: Load configuration during launch phase

This value is distributed into five points of the S/C which are the four down pillars and One for the RTG as shown in figure 9.4.

9.4 CAD Model and Simulation results

A CAD model was implemented with the real dimensions and materials in order to simulate the stresses and show the Structural behavior. The results of the simulations are exported and shown in figure 9.5.

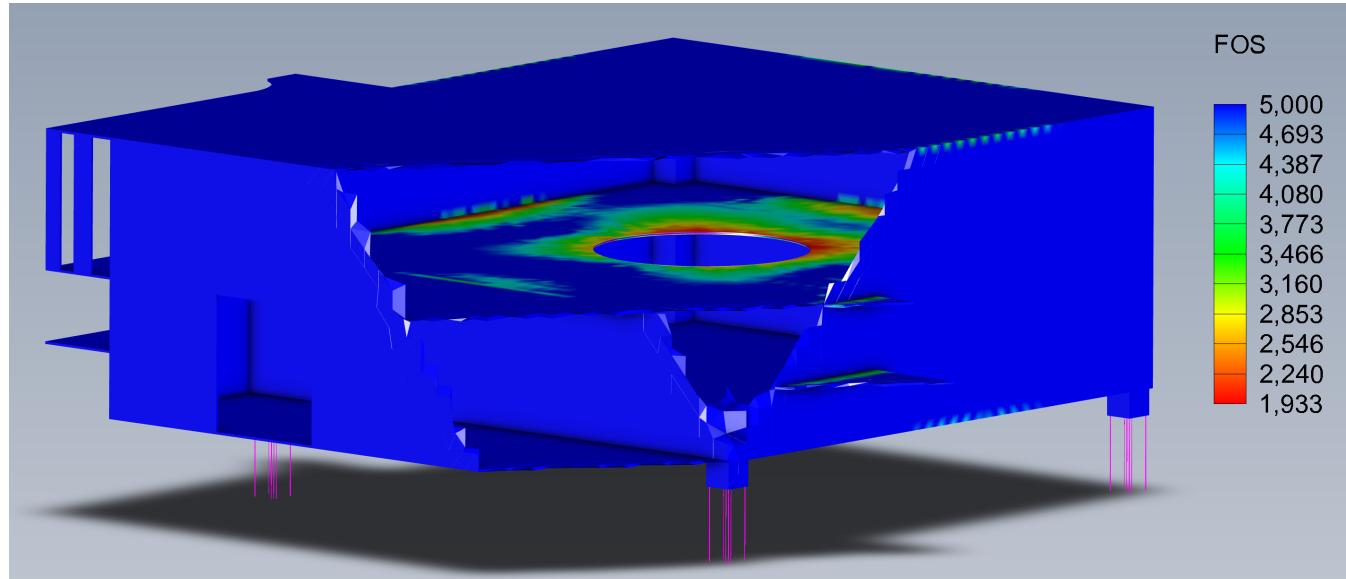


Figure 9.5: Factor of Safety from the FEM analysis

The results show that the critical stress locations (around the tank) have a safety factor of approximately 2 while the other locations are of a 5 or more-safety factor. This is a typical indicator of a non-optimal design, but can be attributed to the fact that this was an approximated simulation which scope was to demonstrate the stress distribution and order of magnitude. In conclusion, it can be said that the structure of the S/C is robust and capable of withstanding all the stresses it will encounter during the mission lifetime.

R Requirements

R.1 Functional

| Req. ID | Description | Related to |
|-----------------|--|---------------|
| ULY-PS-F-010 | The tank shall be at a temperature above the freezing point of hydrazine | ULY-EPS-F-080 |
| ULY-PS-F-020 | The tank shall be in conditions to limit dissociation phenomena of hydrazine | |
| ULY-TTMTC-F-030 | The antennas shall be able to establish a link with the GSs | |
| ULY-AOCS-F-040 | The AOCS shall be able to control the spacecraft | |
| ULY-OBDH-F-050 | The spacecraft shall be able to store data in case of missing link with the GSs | |
| ULY-EPS-F-060 | The spacecraft shall rely on a power source independent from the Sun | |
| ULY-EPS-F-070 | Interference from the RTG shall be minimized | |
| ULY-EPS-F-080 | The RTG shall provide sufficient power in order to fulfill the minimum of 5 years lifetime | |
| ULY-CS-F-090 | The S/C shall withstand all the structural loads that will encounter during the mission | |
| ULY-TCS-F-100 | The S/C shall be able to maintain the temperature of each component in their designated temperature ranges | |

| Req. ID | Description | Related to |
|----------------|--|------------|
| ULY-OBDH-F-110 | The S/C shall acquire and store data almost continuously | |
| ULY-CS-F-120 | The S/C shall fit inside the launcher's dynamic envelope | |
| ULY-CS-F-130 | The S/C's structure should be as light as possible | |

R.2 Operational

| Requirement ID | Description | Related to |
|-----------------|---|-----------------|
| ULY-PS-O-010 | The tank temperature shall be as close as possible to 20 °C | ULY-PS-F-020 |
| ULY-PS-O-020 | The propulsion system shall be restartable | ULY-AOCS-F-040 |
| ULY-PS-O-030 | The propulsion system shall be throttatable | ULY-AOCS-F-040 |
| ULY-AOCS-O-040 | The S/C shall be able to continuously point Earth | ULY-TTMTC-F-030 |
| ULY-TTMTC-O-050 | The HGA shall be able to cover the maximum distance of Ulysses from Earth | ULY-TTMTC-F-030 |
| ULY-TTMTC-O-060 | The HGA shall be able to communicate in both the X-band and S-band | ULY-TTMTC-F-030 |
| ULY-TTMTC-O-070 | The antenna diameter shall be compliant with the spacecraft size | ULY-AOCS-F-040 |

| Requirement ID | Description | Related to |
|----------------|---|---------------|
| ULY-EPS-O-080 | The RTG shall provide an electrical power output greater than 250 W during the nominal mission lifetime | ULY-EPS-F-080 |

R.3 Performance

| Requirement ID | Description | Related to |
|-----------------|--|-----------------|
| ULY-AOCS-P-010 | The pointing error shall be kept below 0.5° | ULY-AOCS-O-040 |
| ULY-TTMTC-P-020 | The SNR shall be higher than 10dB | ULY-TTMTC-F-030 |
| ULY-TTMTC-P-030 | The BER shall be less than 10^{-7} for telemetry | ULY-TTMTC-F-030 |
| ULY-TTMTC-P-040 | The BER shall be less than 10^{-5} for ranging and radio-science | ULY-TTMTC-F-030 |
| ULY-TCS-P-050 | The temperature of hydrazine shall be above of $+5^\circ$ | ULY-TCS-F-100 |
| ULY-TCS-P-060 | The temperature of all experiments solid state detectors shall be above of $+35^\circ$ | ULY-TCS-F-100 |

A Appendix

A.1 Ulysses' Timeline

| Date | Event | Additional details |
|---------------------------|------------------------------------|----------------------------|
| 6 Oct 1990 | Launch | on Space Shuttle Discovery |
| 8 Feb 1992 | Jupiter's closest approach | 6.3 Jovian radii |
| 15 Feb 1992 | 1st Aphelion | 5.40 AU |
| 26 Jun 1994 - 5 Nov 1994 | 1st South Polar Pass | - |
| 12 Mar 1995 | 1st Perihelion | 1.34 AU |
| 19 Jun 1995 - 29 Sep 1995 | 1st North Polar Pass | - |
| 1 May 1996 | C/1996 B2 comet ion tale encounter | - |
| 17 Apr 1998 | 2nd Aphelion | 5.41 AU |
| 1999 | C/2006 P1 comet ion tale encounter | - |
| 6 Sep 2000 - 16 Jan 2001 | 2nd South Polar Pass | - |
| 23 May 2001 | 2nd Perihelion | 1.34 AU |
| 31 Aug 2001 - 10 Dec 2001 | 2nd North Polar Pass | - |
| 30 Jun 2004 | 3rd Aphelion | 5.41 AU |
| 17 Nov 2006 - 3 Apr 2007 | 3rd South Polar Pass | - |
| 5 Feb 2007 - 9 Feb 2007 | C/2006 P1 comet ion tale encounter | - |
| 18 Aug 2007 | 3rd Perihelion | 1.39 AU |
| 30 Nov 2007 - 15 Mar 2008 | 3rd North Polar Pass | - |
| 30 Jun 2009 | Last day of mission operations | - |

Table A.1: Ulysses' timeline

A.2 Payloads' mass, power and data-rate budgets

| Instrument | Mass [kg] | Power [W] | data-rate [bit/s] | Additional details |
|-------------------|------------------|------------------|--------------------------|---|
| COSPIN | 14.6 | 14.7 | 160 | |
| DUST | 3.8 | 2.2 | 8 | |
| EPAC/GAS | 4.3 | 4.1 | 16 | |
| FGM/VHM | 4.7 | 5.4 | 40/80 | 40 bit/s in cruise mode 80 bit/s in tracking mode |
| GRB | 2.0 | 2.6 | 20/40 | 20 bit/s in cruise mode 40 bit/s in tracking mode |
| HI-SCALE | 5.775 | 4.0 | 80/160 | 80 bit/s in cruise mode 160 bit/s in tracking mode |
| SWICS | 5.4769 | 3.78 | 44/88 | 44 bit/s in cruise mode 88 bit/s in tracking mode |
| SWOOPS | 6.7 | 5.5 | 160 | |
| URAP | 7.4 | 10 | 232 | mass considered excluding antennas |
| GWE | NA | NA | NA | |
| SCE | NA | NA | NA | |

Table A.2: Payloads brief description

A.3 Ulysses' trajectory from ephemerides

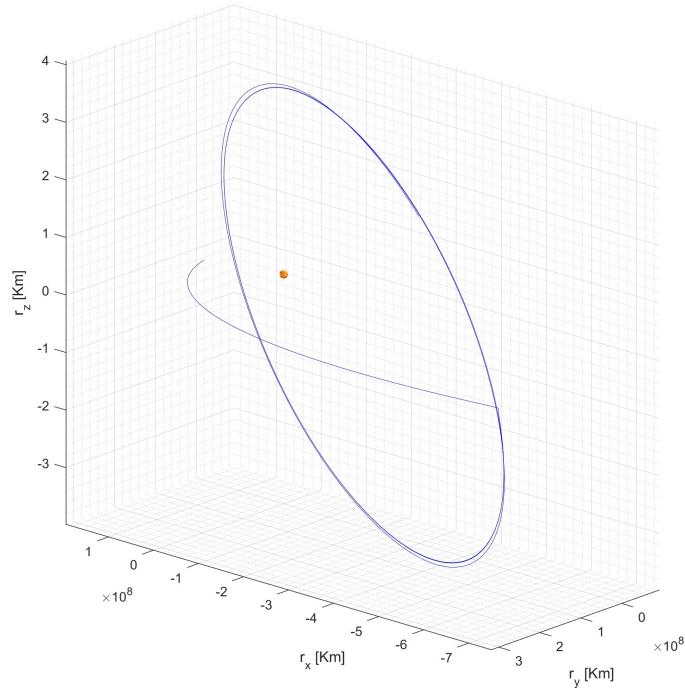


Figure A.1: Trajectory extrapolated from Ulysses' ephemerides from 1990-10-07 to 2009-06-30

A.4 Parking orbit and injection into the transfer to Jupiter

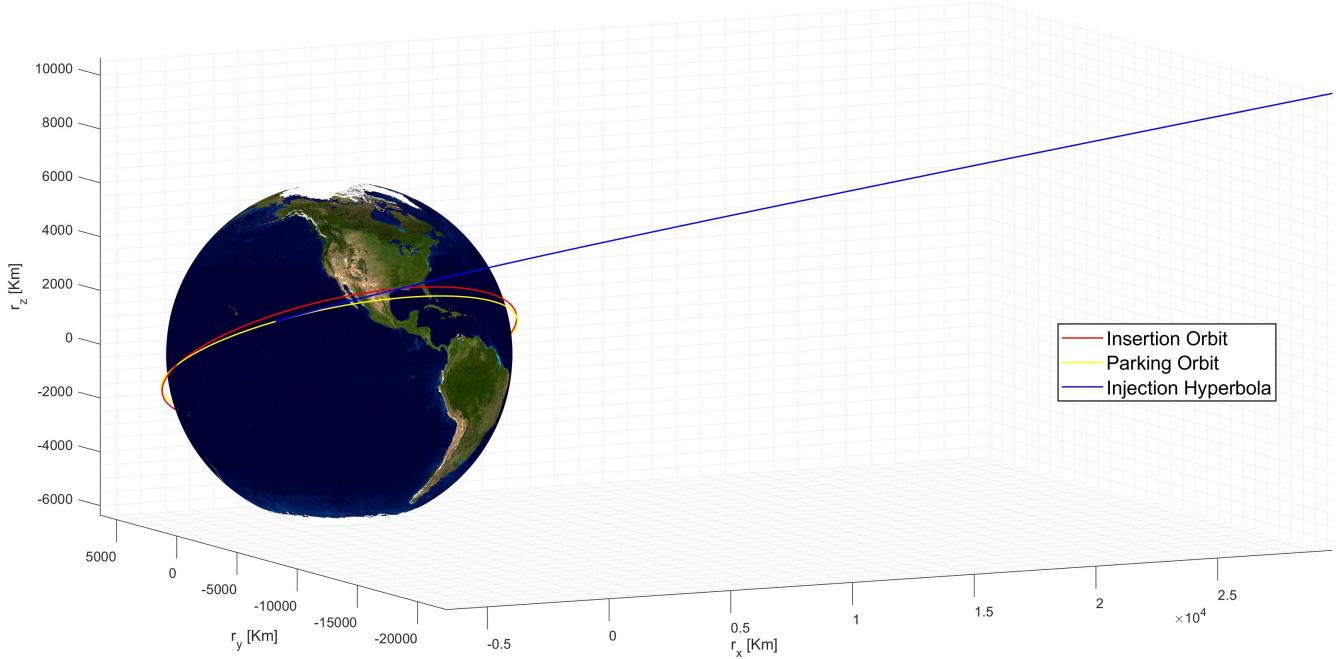


Figure A.2: Parking orbit and injection into the transfer to Jupiter

A.5 Earth-Jupiter transfer

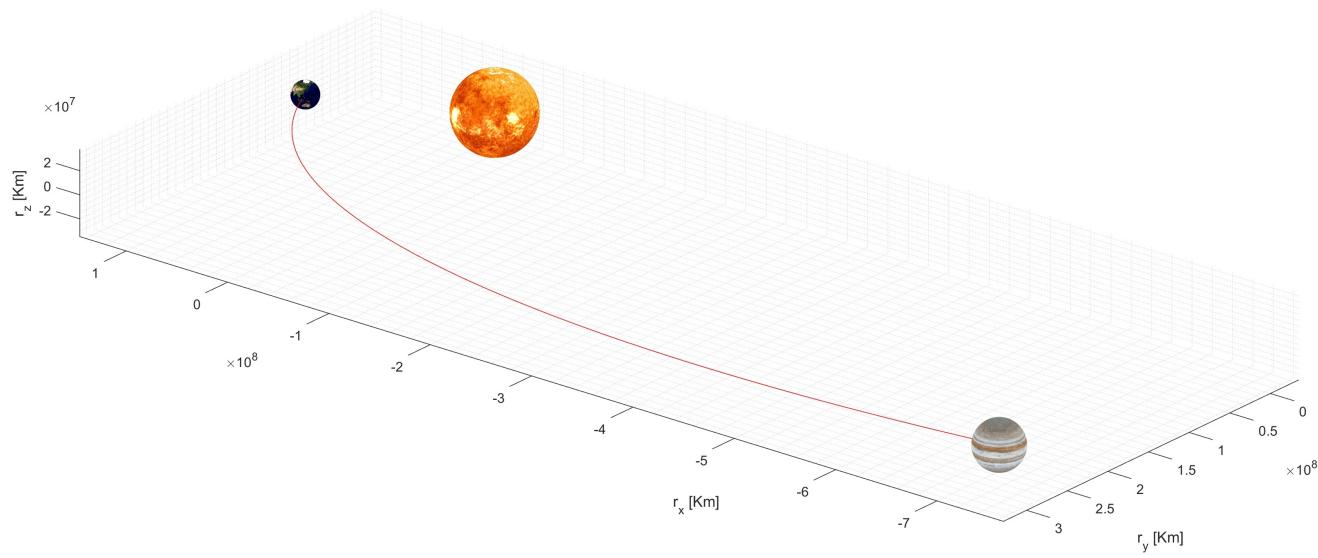


Figure A.3: Earth-Jupiter transfer trajectory

A.6 Jupiter's flyby trajectory

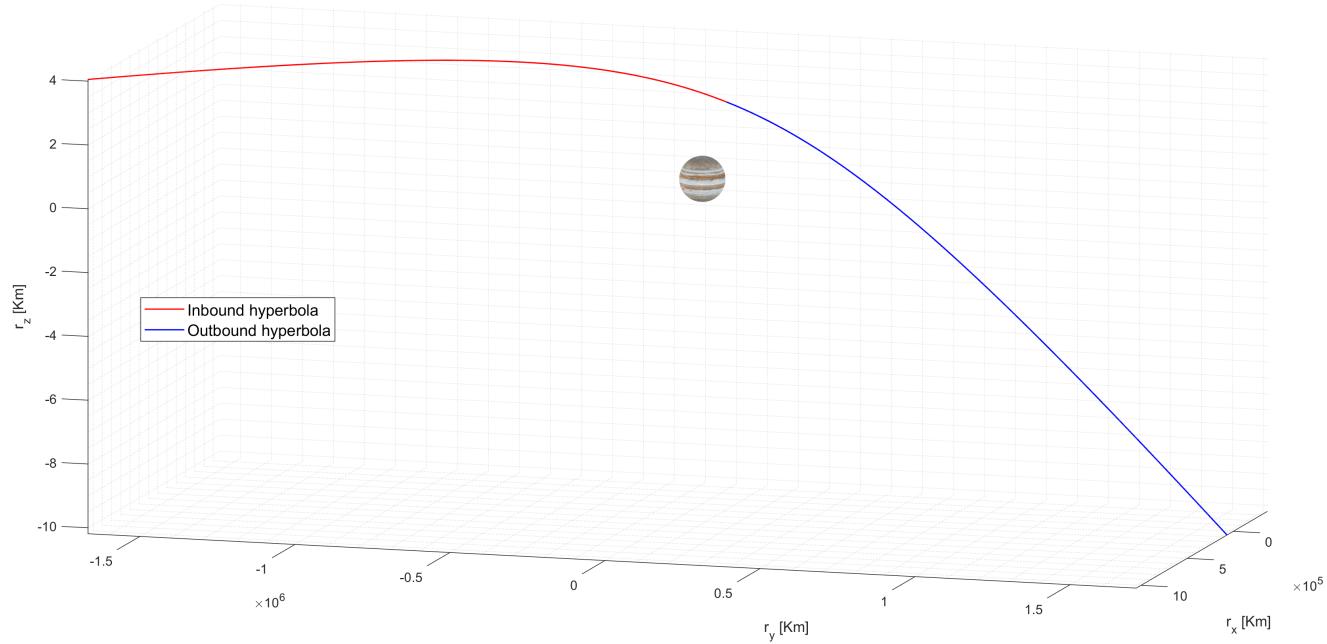


Figure A.4: Jupiter's flyby trajectory

A.7 Mars flyby alternative

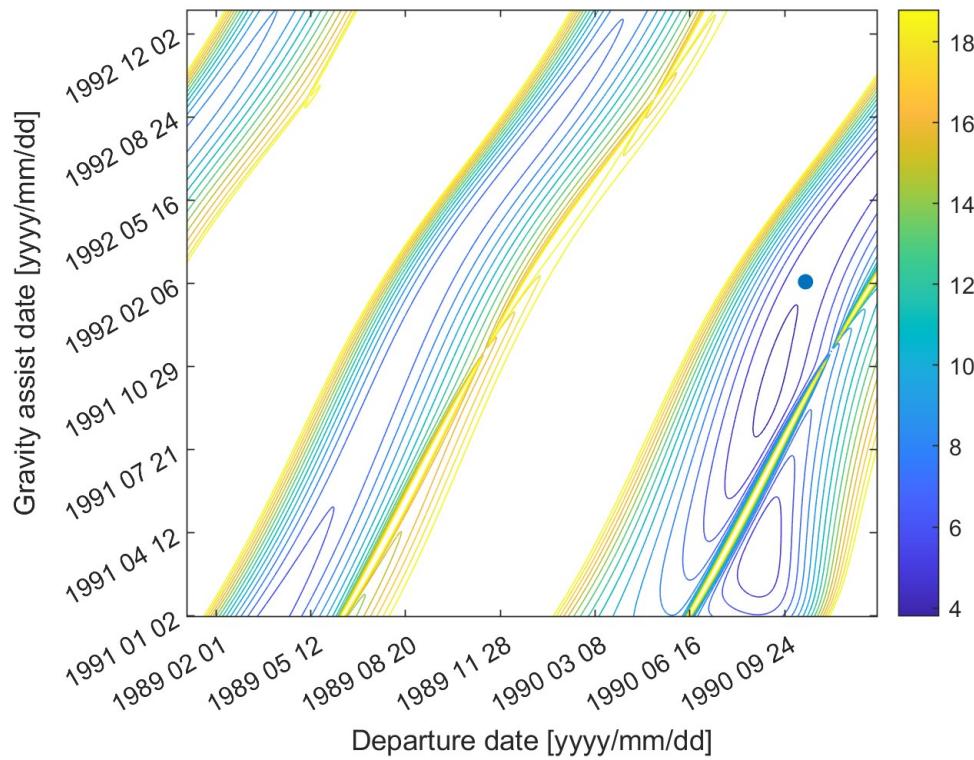


Figure A.5: Pork-chop plot for hypothetical Earth-Mars arc

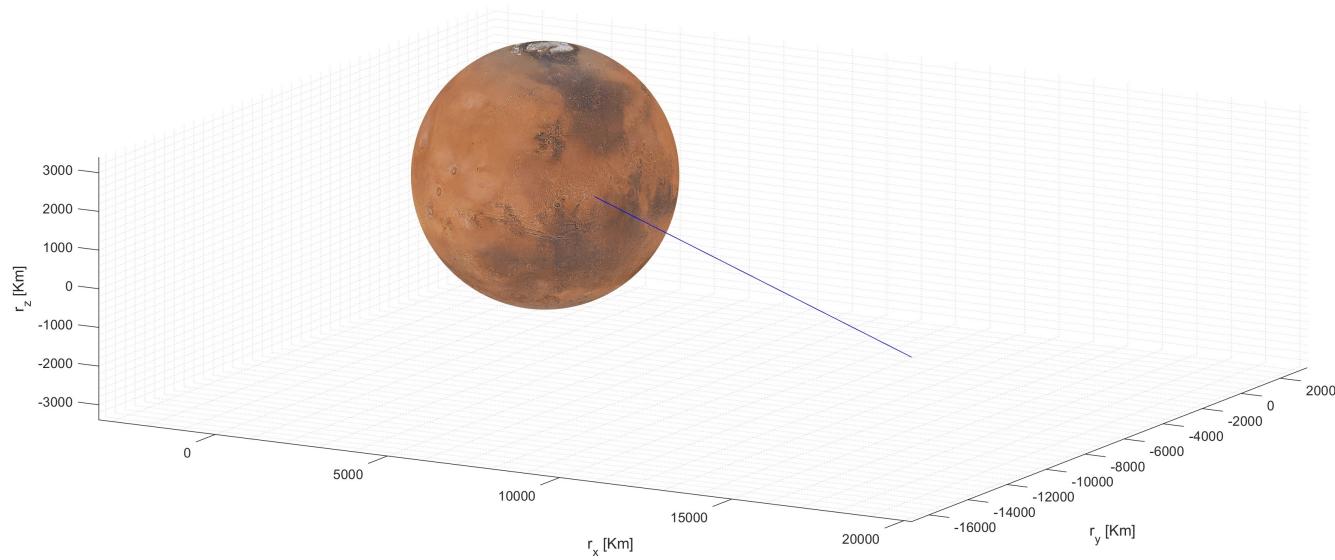


Figure A.6: Hypothetical Mars' flyby

A.8 Propellant mass and tank's temperature variability with time

| Date | Propellant [kg] | Temperature [°C] |
|----------|-----------------|------------------|
| Oct 1990 | 33.491 | 24.30 |
| Nov 1990 | 15.473 | 20.47 |
| Feb 1991 | 14.690 | 25.44 |
| Mar 1991 | 14.655 | 25.86 |
| Feb 1992 | 14.322 | 25.03 |
| Mar 1994 | 13.759 | 22.54 |
| Apr 1995 | 12.459 | 19.20 |
| Jan 1996 | 11.617 | 21.30 |
| Jan 1998 | 11.046 | 14.84 |
| Jan 2004 | 7.930 | 10.60 |
| Jan 2005 | 7.728 | 10.24 |
| Jun 2009 | 0.750 | 11.89 |

Table A.3: Propellant mass stored and tank temperature during Ulysses' lifetime

A.9 Antennas position

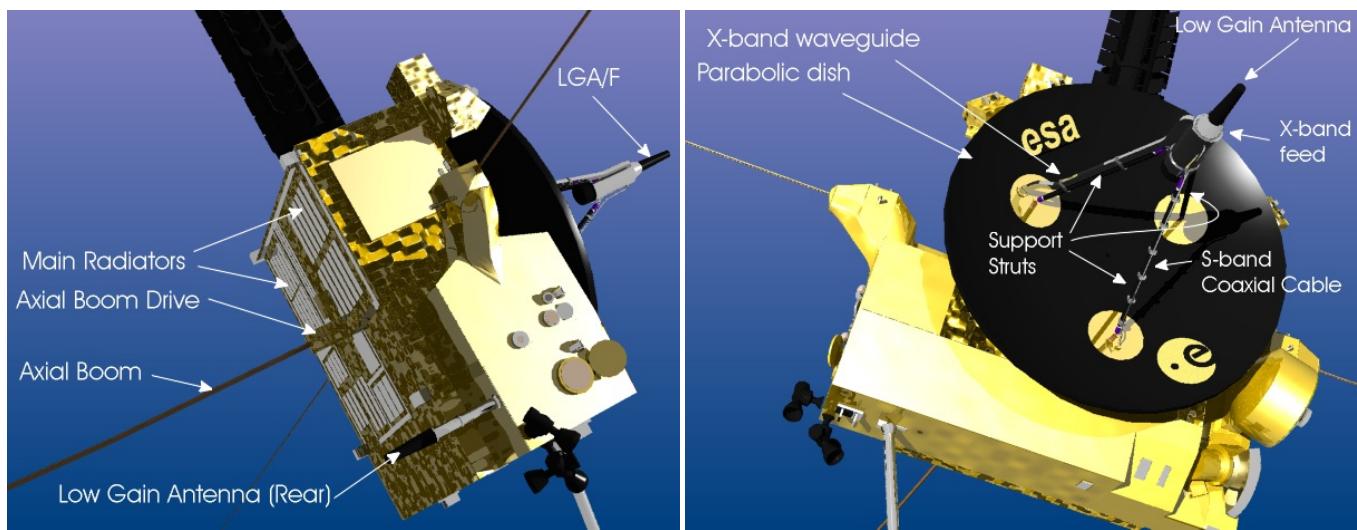


Figure A.7: Antennas summary

A.10 Conjunctions and oppositions summary

| Conjunction | Date | SPE [deg] | SEP [deg] | Scientific Activity |
|-------------|-------------|--------------|--------------|---------------------|
| 1st | 21 Aug 1991 | 0.4 | 1.2 | Prime SCE |
| 2nd | 2 Sep 1992 | 1.5 | 7.8 | Secondary SCE |
| 3rd | 3 Sep 1993 | 5.8 | 25.6 | Routine |
| 4th | 4 Mar 1995 | 4.3 | 5.8 | Routine |
| 5th | 30 Aug 1997 | 2.0 | 10.5 | Routine |
| 6th | 1 Sep 1998 | 0.9 | 4.8 | Routine |
| 7th | 5 Sep 1999 | 4.6 | 21.6 | Routine |

Table A.4: Conjunctions timeline

| Opposition | Date | SPE [deg] | SEP [deg] | Scientific Activity |
|------------|-------------|--------------|--------------|---------------------|
| 1st | 30 Dec 1990 | 3.4 | 174.6 | Test GWE |
| 2nd | 27 Feb 1992 | 0.1 | 179.4 | Primary GWE |
| 3rd | 1 Mar 1993 | 4.6 | 156.4 | Routine |
| 4th | 24 Feb 1997 | 5.6 | 151.6 | Routine |
| 5th | 26 Feb 1998 | 0.8 | 175.7 | MIDAS |
| 6th | 1 Mar 1999 | 3.5 | 161.5 | Routine |

Table A.5: Opposition timeline

A.11 Antennas diameters sizing

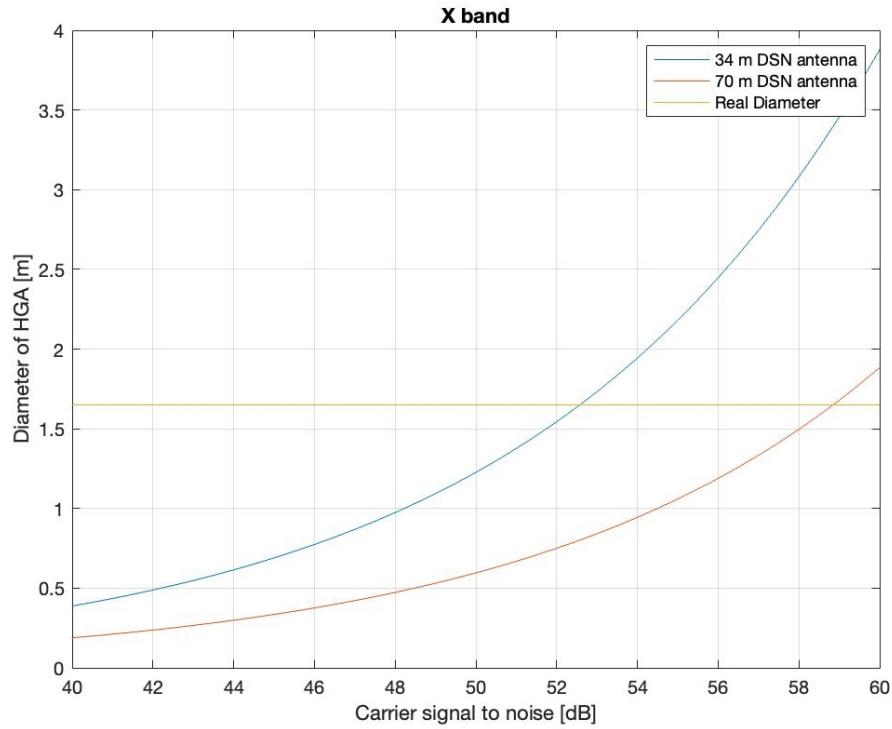


Figure A.8: Diameter of the HGA with respect to the carrier signal to noise for the communication with DSN in the X band

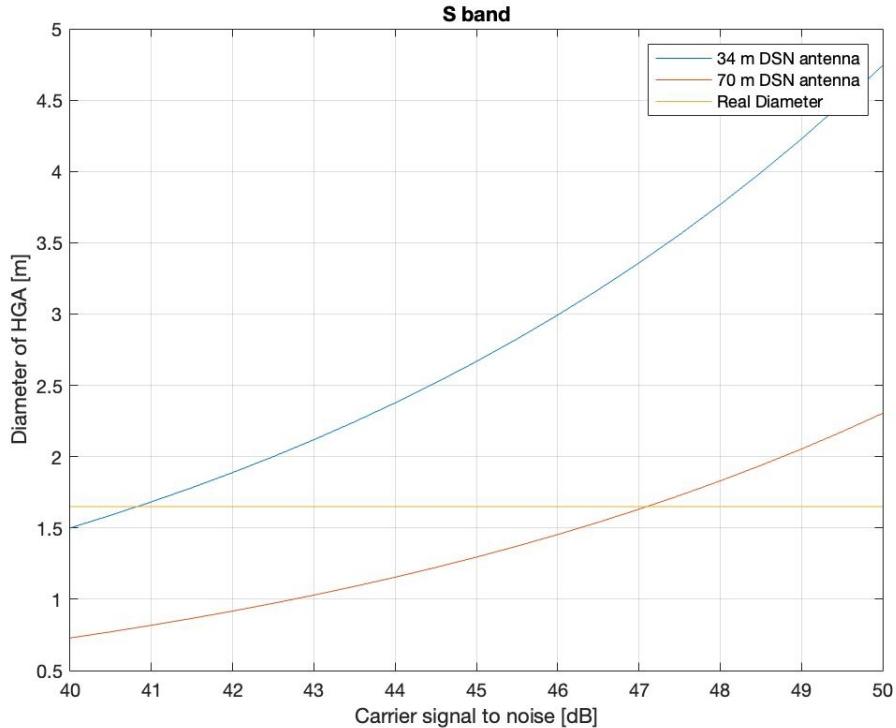


Figure A.9: Diameter of the HGA with respect to the carrier signal to noise for the communication with DSN in the S-band

A.12 DSN coverage

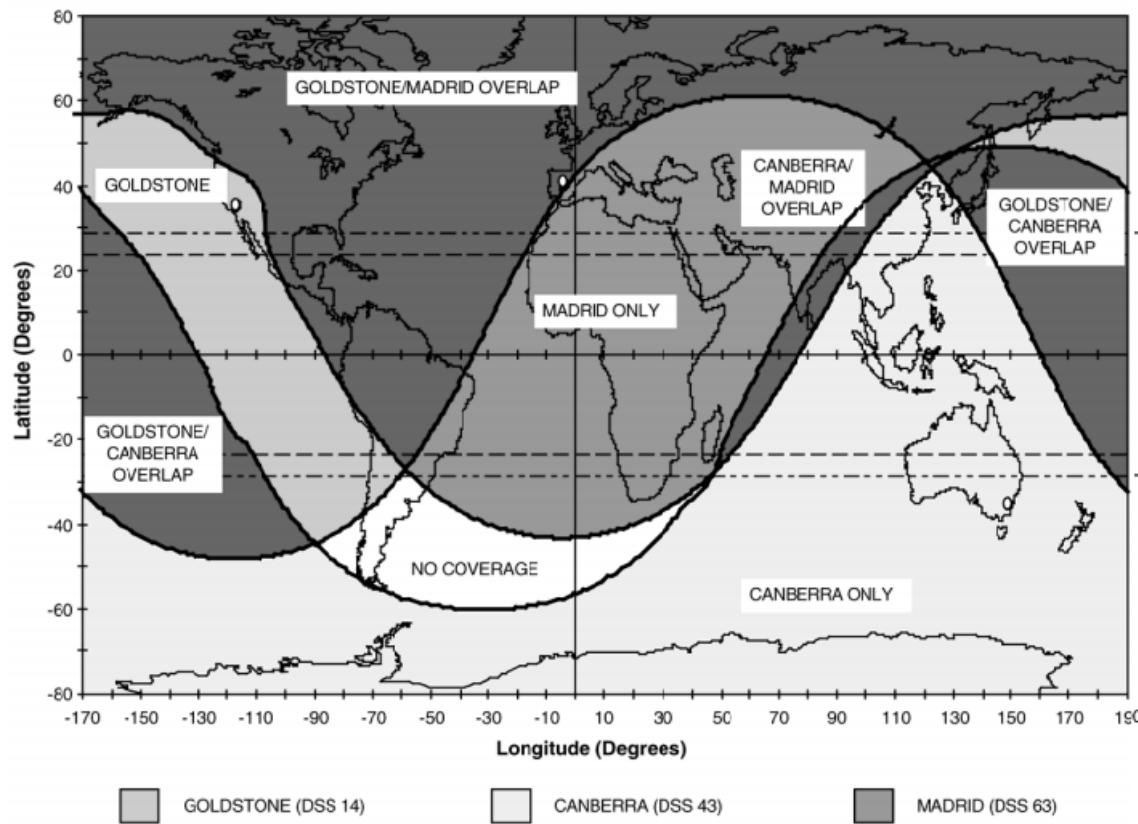


Figure A.10: DSN coverage

A.13 Radioisotopes characteristics

| Isotope | Fuel form | Half-life [years] | Power density [W/g] | Shielding |
|-------------------|-------------------------|-------------------|---------------------|-----------|
| ^{238}Pu | PuO_2 | 87.7 | 0.41 | Low |
| ^{90}Sr | SrO | 28.8 | 0.46 | High |
| ^{210}Po | GdPo | 0.378 | 140 | Low |
| ^{241}Am | Am_2O_3 | 432 | 0.144 | Medium |
| ^{242}Cu | Cu_2O_3 | 0.4 | 98 | Low |

Table A.6: Different radioisotopes characteristics

A.14 Eclipse from Jupiter

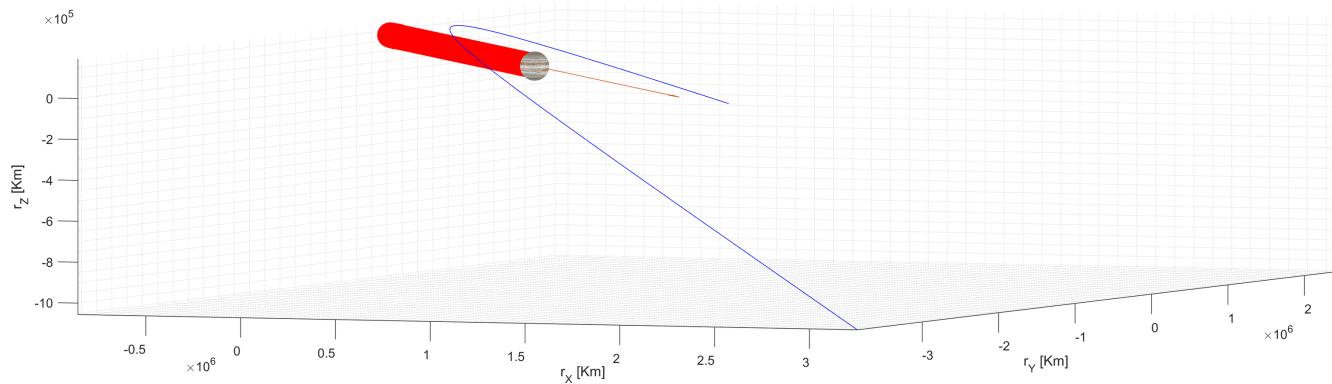


Figure A.11: Eclipse from Jupiter analysis

A.15 External configuration of the spacecraft

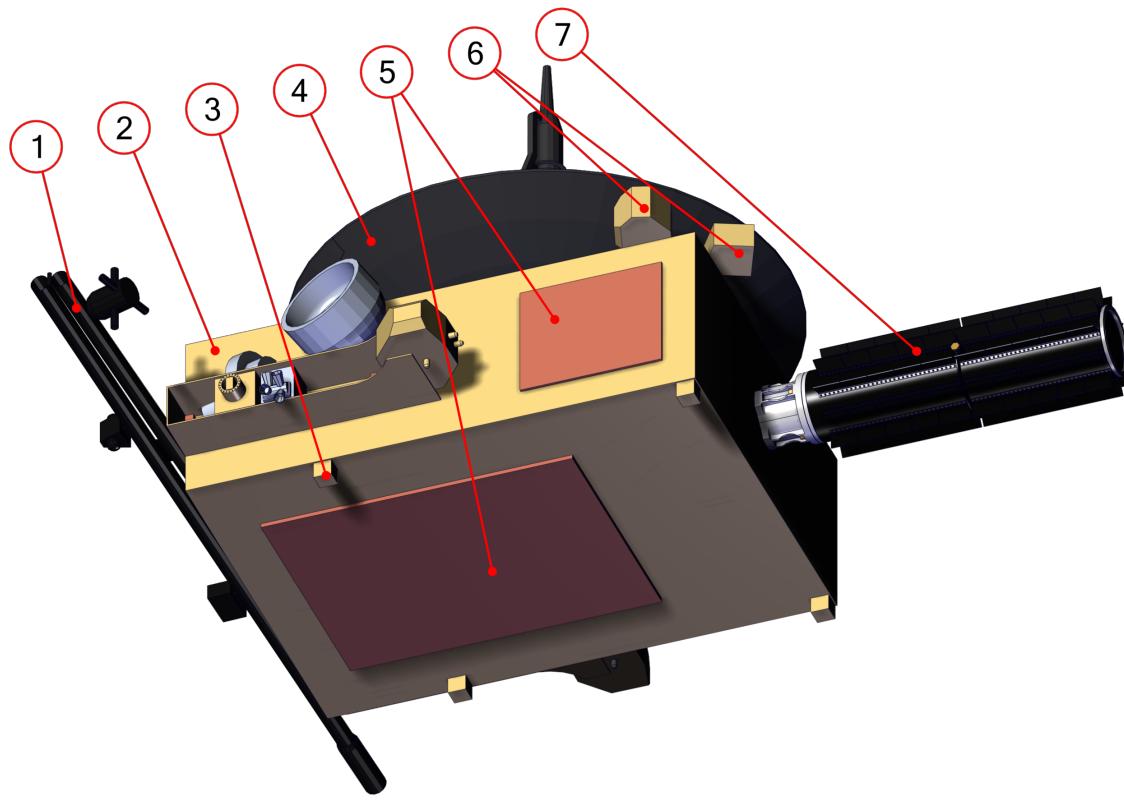


Figure A.12: Configuration of the external space of the S/C

A.16 Upper and lower case configuration

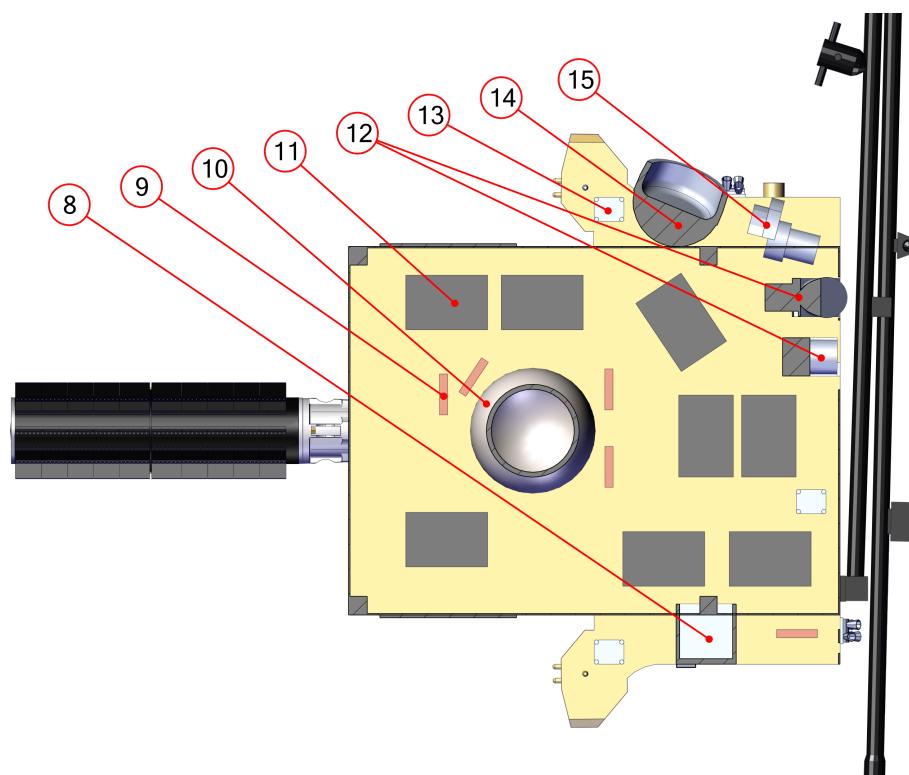


Figure A.13: Configuration of the upper shelf of the case

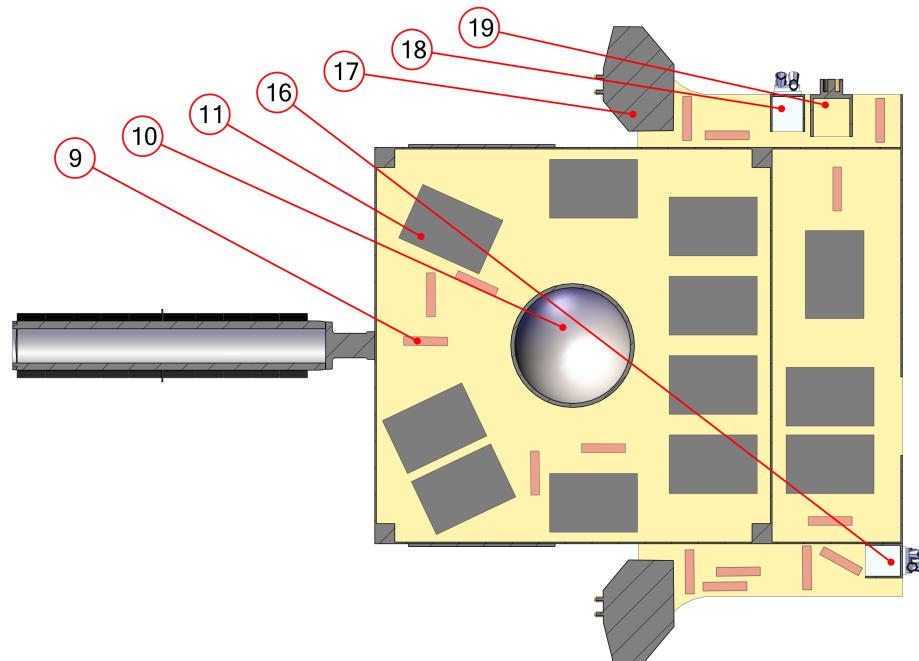


Figure A.14: Configuration of the lower shelf of the case

A.17 Bill of materials of figures A.12, A.13 and A.14

| Callout | Name | Quantity |
|---------|-------------------------|----------|
| 1 | Radial Boom | 1 |
| 2 | Structural Case | 1 |
| 3 | Longeron | 4 |
| 4 | High-Gain Antenna | 1 |
| 5 | External Power Dumpers | 3 |
| 6 | Sun Sensors | 4 |
| 7 | RTG | 1 |
| 8 | COSPIN | 1 |
| 9 | IPDs and Heater Drivers | 20 |
| 10 | Hydrazine Tank | 1 |
| 11 | Electronic Units | 20 |
| 12 | SWOOPS | 2 |
| 13 | URAP | 4 |
| 14 | DUST | 1 |
| 15 | SWICS | 1 |
| 16 | HI-Scale | 1 |
| 17 | Thrusters Block | 2 |
| 18 | EPAC | 1 |
| 19 | GAS | 1 |

Table A.7: Bill of materials of figures A.12, A.13 and A.14

References

- [1] NASA. *Space Shuttle Reference Manual*. 1988.
- [2] John F McCarthy. “Zero g Propulsion Problems”. In: *Jet, Rocket, Nuclear, Ion and Electric Propulsion*. Springer, 1968, pp. 644–727.
- [3] Andrew McGarry, William Berry, and David Parker. “In Flight Performance of the Ulysses Reaction Control System”. In: *European Spacecraft Propulsion Conference*. Vol. 398. 1997, p. 93.
- [4] Obadiah Kegege et al. “Three-dimensional analysis of Deep Space Network antenna coverage”. In: *2012 IEEE Aerospace Conference*. IEEE. 2012, pp. 1–9.
- [5] CK Chan, ES Paredes, and MS Ryne. “Ulysses Attitude and Orbit Operations: 13+ Years of International Cooperation”. In: *Space OPS 2004 Conference*. 2004, p. 447.
- [6] F Landis Markley and John L Crassidis. “Fundamentals of spacecraft attitude determination and control”. In: (2014).
- [7] Jong-Hoon Won, Sun-Jun Ko, and Ja-Sung Lee. “New Quaternion-based Least-squares Method for Attitude Determination with Vector Observations”. In: () .
- [8] KP Wenzel et al. “The Ulysses mission”. In: *Astronomy and Astrophysics Supplement Series* 92 (1992), p. 207.
- [9] V Raag. *Performance characteristics of a silicon-germanium RTG in long-term operation*. Tech. rep. 1969.
- [10] NASA Johnson Space Center. “Space Shuttle Program Payload Bay Payload User’s Guide”. In: *Space* (2000).
- [11] Shuttle Orbiter and Cargo Standard Interfaces. “ICD 2-19001”. In: *Revision K* (1993).